The Astrophysical Journal Letters, 902:L21 (17pp), 2020 October 10 https://doi.org/10.3847/2041-8213/abb655

Gravitational-wave Constraints on the Equatorial Ellipticity of Millisecond Pulsars

R. Abbott[1], T. D. Abbott[2], S. Abraham[3], F. Acernese[4,5], K. Ackley[6], A. Adams[7], C. Adams[8], R. X. Adhikari[1], V. B. Adya[9], C. Affeldt[10,11], M. Agathos[12,13], K. Agatsuma[14], N. Aggarwal[15], O. D. Aguiar[16], L. Aiello[17,18], A. Ain[19,20], P. Ajith[21], G. Allen[22], A. Allocca[19], P. A. Altin[9], A. Amato[23], S. Anand[1], A. Ananyeva[1], S. B. Anderson[1], W. G. Anderson[24], S. V. Angelova[25], S. Ansoldi[26,27], J. M. Antelis[28], S. Antier[29], S. Appert[1], K. Arai[1], M. C. Araya[1], J. S. Areeda[30], M. Arène[29], N. Arnaud[31,32], S. M. Aronson[33], K. G. Arun[34], Y. Asali[35], S. Ascenzi[17,36], G. Ashton[6], S. M. Aston[8], P. Astone[37], F. Aubin[38], P. Aufmuth[10,11], K. AultONeal[28], C. Austin[2], V. Avendano[39], S. Babak[29], F. Badaracco[17,18], M. K. M. Bader[40], S. Bae[41], A. M. Baer[7], S. Bagnasco[42], M. Bailes[43], J. Baird[29], M. Ball[44], G. Ballardin[32], S. W. Ballmer[45], A. Bals[28], A. Balsamo[7], G. Baltus[46], S. Banagiri[47], D. Bankar[3], R. S. Bankar[3], J. C. Barayoga[1], C. Barbieri[48,49,50], B. C. Barish[1], D. Barker[51], P. Barneo[52], S. Barnum[53], F. Barone[5,54], B. Barr[55], L. Barsotti[53], M. Barsuglia[29], D. Barta[56], J. Bartlett[51], I. Bartos[33], R. Bassiri[57], A. Basti[19,20], M. Bawaj[58,59], J. C. Bayley[55], M. Bazzan[60,61], B. R. Becher[62], B. Bécsy[63], V. M. Bedakihale[64], M. Bejger[65], I. Belahcene[31], D. Beniwal[66], M. G. Benjamin[28], T. F. Bennett[67], J. D. Bentley[14], F. Bergamin[10,11], B. K. Berger[57], G. Bergmann[10,11], S. Bernuzzi[13], D. Bersanetti[68], A. Bertolini[40], J. Betzwieser[8], R. Bhandare[69], A. V. Bhandari[3], D. Bhattacharjee[70], J. Bidler[30], I. A. Bilenko[71], G. Billingsley[1], R. Birney[72], O. Birnholtz[73], S. Biscans[1,53], M. Bischi[74,75], S. Biscoveanu[53], A. Bisht[10,11], M. Bitossi[19,32], M.-A. Bizouard[76], J. K. Blackburn[1], J. Blackman[77], C. D. Blair[78], D. G. Blair[78], R. M. Blair[51], O. Blanch[79], F. Bobba[80,81], N. Bode[10,11], M. Boer[76], Y. Boetzel[82], G. Bogaert[76], M. Boldrini[37,83], F. Bondu[84], R. Bonnand[38], P. Booker[10,11], B. A. Boom[40], R. Bork[1], V. Boschi[19], S. Bose[3], V. Bossilkov[78], V. Boudart[46], Y. Bouffanais[60,61], A. Bozzi[32], C. Bradaschia[19], P. R. Brady[24], A. Bramley[8], M. Branchesi[17,18], J. E. Brau[44], M. Breschi[13], T. Briant[85], J. H. Briggs[55], F. Brighenti[74,75], A. Brillet[76], M. Brinkmann[10,11], P. Brockill[24], A. F. Brooks[1], J. Brooks[32], D. D. Brown[66], S. Brunett[1], G. Bruno[86], R. Bruntz[7], A. Buikema[53], T. Bulik[87], H. J. Bulten[40,88], A. Buonanno[89,90], D. Buskulic[38], R. L. Byer[57], M. Cabero[10,11], L. Cadonati[91], M. Caesar[92], G. Cagnoli[23], C. Cahillane[1], J. Calderón Bustillo[6], J. D. Callaghan[55], T. A. Callister[93], E. Calloni[5,94], J. B. Camp[95], M. Canepa[68,96], K. C. Cannon[97], H. Cao[66], J. Cao[98], G. Carapella[80,81], F. Carbognani[32], M. F. Carney[15], M. Carpinelli[99,100], G. Carullo[19,20], T. L. Carver[101], J. Casanueva Diaz[32], C. Casentini[36,102], S. Caudill[40], M. Cavaglià[70], F. Cavalier[31], R. Cavalieri[32], G. Cella[19], P. Cerdá-Durán[103], E. Cesarini[36], W. Chaibi[76], K. Chakravarti[3], C.-L. Chan[104], C. Chan[97], K. Chandra[105], P. Chanial[32], S. Chao[106], P. Charlton[107], E. A. Chase[15], E. Chassande-Mottin[29], D. Chatterjee[24], M. Chaturvedi[69], A. Chen[104], H. Y. Chen[108], X. Chen[78], Y. Chen[77], H.-P. Cheng[33], C. K. Cheong[104], H. Y. Chia[33], F. Chiadini[81,109], R. Chierici[110], A. Chincarini[68], A. Chiummo[32], G. Cho[111], H. S. Cho[112], M. Cho[90], S. Choate[92], N. Christensen[76], Q. Chu[78], S. Chua[85], K. W. Chung[113], S. Chung[78], G. Ciani[60,61], P. Ciecielag[65], M. Cieślar[65], M. Cifaldi[36,102], A. A. Ciobanu[66], R. Ciolfi[61,114], F. Cipriano[76], A. Cirone[68,96], F. Clara[51], E. N. Clark[115], J. A. Clark[91], L. Clarke[116], P. Clearwater[117], S. Clesse[86], F. Cleva[76], E. Coccia[17,18], P.-F. Cohadon[85], D. E. Cohen[31], M. Colleoni[118], C. G. Collette[119], C. Collins[14], M. Colpi[48,49], M. Constancio, Jr.[16], L. Conti[61], S. J. Cooper[14], P. Corban[8], T. R. Corbitt[2], I. Cordero-Carrión[120], S. Corezzi[58,59], K. R. Corley[35], N. Cornish[63], D. Corre[31], A. Corsi[121], S. Cortese[32], C. A. Costa[16], R. Cotesta[89], M. W. Coughlin[1,47], S. B. Coughlin[15,101], J.-P. Coulon[76], S. T. Countryman[35], P. Couvares[1], P. B. Covas[118], D. M. Coward[78], M. J. Cowart[8], D. C. Coyne[1], R. Coyne[122], J. D. E. Creighton[24], T. D. Creighton[123], M. Croquette[85], S. G. Crowder[124], J. R. Cudell[46], T. J. Cullen[2], A. Cumming[55], R. Cummings[55], L. Cunningham[55], E. Cuoco[32,125], M. Curylo[87], T. Dal Canton[31,89], G. Dálya[126], A. Dana[57], L. M. DaneshgaranBajastani[67], B. D'Angelo[68,96], S. L. Danilishin[127], S. D'Antonio[36], K. Danzmann[10,11], C. Darsow-Fromm[128], A. Dasgupta[64], L. E. H. Datrier[55], V. Dattilo[32], I. Dave[69], M. Davier[31], G. S. Davies[129], D. Davis[1], E. J. Daw[130], R. Dean[92], D. DeBra[57], M. Deenadayalan[3], J. Degallaix[131], M. De Laurentis[5,94], S. Deléglise[85], V. Del Favero[132], N. De Lillo[55], W. Del Pozzo[19,20], L. M. DeMarchi[15], F. De Matteis[36,102], V. D'Emilio[101], N. Demos[53], T. Denker[10,11], T. Dent[129], A. Depasse[86], R. De Pietri[133,134], R. De Rosa[5,94], C. De Rossi[32], R. DeSalvo[81,135], O. de Varona[10,11], S. Dhurandhar[3], M. C. Díaz[123], M. Diaz-Ortiz, Jr.[33], N. A. Didio[45], T. Dietrich[40], L. Di Fiore[5], C. DiFronzo[14], C. Di Giorgio[80,81], F. Di Giovanni[103], M. Di Giovanni[136,137], T. Di Girolamo[5,94], A. Di Lieto[19,20], B. Ding[119], S. Di Pace[37,83], I. Di Palma[37,83], F. Di Renzo[19,20], A. K. Divakarla[33], A. Dmitriev[14], Z. Doctor[44], L. D'Onofrio[5,94], F. Donovan[53], K. L. Dooley[101], S. Doravari[3], I. Dorrington[101], T. P. Downes[24], M. Drago[17,18], J. C. Driggers[51], Z. Du[98], J.-G. Ducoin[31], P. Dupej[55], O. Durante[80,81], D. D'Urso[99,100], P.-A. Duverne[31], S. E. Dwyer[51], P. J. Easter[6], G. Eddolls[55], B. Edelman[44], T. B. Edo[130], O. Edy[138], A. Effler[8], J. Eichholz[9], S. S. Eikenberry[33], M. Eisenmann[38], R. A. Eisenstein[53], A. Ejlli[101], L. Errico[5,94], R. C. Essick[108], H. Estellés[118], D. Estevez[38], Z. B. Etienne[139], T. Etzel[1], M. Evans[53], T. M. Evans[8], B. E. Ewing[140], V. Fafone[17,36,102], H. Fair[45], S. Fairhurst[101], X. Fan[98], A. M. Farah[108], S. Farinon[68], B. Farr[44], W. M. Farr[93,141], E. J. Fauchon-Jones[101], M. Favata[39], M. Fays[46,130], M. Fazio[142], J. Feicht[1], M. M. Fejer[57], F. Feng[29], E. Fenyvesi[56,143], D. L. Ferguson[91], A. Fernandez-Galiana[53], I. Ferrante[19,20], T. A. Ferreira[16], F. Fidecaro[19,20], P. Figura[87], I. Fiori[32], D. Fiorucci[17,18], M. Fishbach[108], R. P. Fisher[7], J. M. Fishner[53], R. Fittipaldi[81,144], M. Fitz-Axen[47], V. Fiumara[81,145], R. Flaminio[38,146], E. Floden[47], E. Flynn[30], H. Fong[97], J. A. Font[103,147], P. W. F. Forsyth[9], J.-D. Fournier[76], S. Frasca[37,83], F. Frasconi[19], Z. Frei[126], A. Freise[14], R. Frey[44], V. Frey[31], P. Fritschel[53], V. V. Frolov[8], G. G. Fronzé[42], P. Fulda[33], M. Fyffe[8], H. A. Gabbard[55], B. U. Gadre[89], S. M. Gaebel[14], J. R. Gair[89], J. Gais[104], S. Galaudage[6], R. Gamba[13], D. Ganapathy[53], A. Ganguly[21], S. G. Gaonkar[3], B. Garaventa[68,96], C. García-Quirós[118], F. Garufi[5,94], B. Gateley[51], S. Gaudio[28], V. Gayathri[33], G. Gemme[68], A. Gennai[19],

D. George[22], J. George[69], L. Gergely[148], S. Ghonge[91], Abhirup Ghosh[89], Archisman Ghosh[40,149,150,151], S. Ghosh[24,39], B. Giacomazzo[48,49,50], L. Giacoppo[37,83], J. A. Giaime[2,8], K. D. Giardina[8], D. R. Gibson[72], C. Gier[25], K. Gill[35], P. Giri[19,20], J. Glanzer[2], A. E. Gleckl[30], P. Godwin[140], E. Goetz[152], R. Goetz[33], N. Gohlke[10,11], B. Goncharov[6], G. González[2], A. Gopakumar[153], S. E. Gossan[1], M. Gosselin[19,20], R. Gouaty[38], B. Grace[9], A. Grado[5,154], M. Granata[131], V. Granata[80], A. Grant[55], S. Gras[53], P. Grassia[1], C. Gray[51], R. Gray[55], G. Greco[74,75], A. C. Green[33], R. Green[101], E. M. Gretarsson[28], H. L. Griggs[91], G. Grignani[58,59], A. Grimaldi[136,137], E. Grimes[28], S. J. Grimm[17,18], H. Grote[101], S. Grunewald[89], P. Gruning[31], J. G. Guerrero[30], G. M. Guidi[74,75], A. R. Guimaraes[2], G. Guixé[52], H. K. Gulati[64], Y. Guo[40], Anchal Gupta[1], Anuradha Gupta[140], P. Gupta[40,155], E. K. Gustafson[1], R. Gustafson[156], F. Guzman[115], L. Haegel[29], O. Halim[17,18], E. D. Hall[53], E. Z. Hamilton[101], G. Hammond[55], M. Haney[82], M. M. Hanke[10,11], J. Hanks[51], C. Hanna[140], M. D. Hannam[101], O. A. Hannuksela[104], O. Hannuksela[40,155], H. Hansen[51], T. J. Hansen[28], J. Hanson[8], T. Harder[76], T. Hardwick[2], K. Haris[21,40,155], J. Harms[17,18], G. M. Harry[157], I. W. Harry[138], D. Hartwig[128], R. K. Hasskew[8], C.-J. Haster[53], K. Haughian[55], F. J. Hayes[55], J. Healy[132], A. Heidmann[85], M. C. Heintze[8], J. Heinze[10,11], J. Heinzel[158], H. Heitmann[76], F. Hellman[159], P. Hello[31], A. F. Helmling-Cornell[44], G. Hemming[32], M. Hendry[55], I. S. Heng[55], E. Hennes[40], J. Hennig[10,11], M. H. Hennig[10,11], F. Hernandez Vivanco[6], M. Heurs[10,11], S. Hild[127], P. Hill[25], A. S. Hines[115], S. Hochheim[10,11], E. Hofgard[57], D. Hofman[131], J. N. Hohmann[128], A. M. Holgado[22], N. A. Holland[9], I. J. Hollows[130], Z. J. Holmes[66], K. Holt[8], D. E. Holz[108], P. Hopkins[101], C. Horst[24], J. Hough[55], E. J. Howell[78], C. G. Hoy[101], D. Hoyland[14], Y. Huang[53], M. T. Hübner[6], A. D. Huddart[116], E. A. Huerta[22], B. Hughey[28], V. Hui[38], S. Husa[118], S. H. Huttner[55], B. M. Hutzler[2], R. Huxford[140], T. Huynh-Dinh[8], B. Idzkowski[87], A. Iess[36,102], S. Imperato[15], H. Inchauspe[33], C. Ingram[66], G. Intini[37,83], M. Isi[53], B. R. Iyer[21], V. JaberianHamedan[78], T. Jacqmin[85], S. J. Jadhav[160], S. P. Jadhav[3], A. L. James[101], K. Jani[91], K. Janssens[161], N. N. Janthalur[160], P. Jaranowski[162], D. Jariwala[33], R. Jaume[118], A. C. Jenkins[113], M. Jeunon[47], J. Jiang[33], G. R. Johns[7], A. W. Jones[14], D. I. Jones[163], J. D. Jones[51], P. Jones[14], R. Jones[55], R. J. G. Jonker[40], L. Ju[78], J. Junker[10,11], C. V. Kalaghatgi[101], V. Kalogera[15], B. Kamai[1], S. Kandhasamy[3], G. Kang[41], J. B. Kanner[1], S. J. Kapadia[21], D. P. Kapasi[9], C. Karathanasis[79], S. Karki[70], R. Kashyap[140], M. Kasprzack[1], W. Kastaun[10,11], S. Katsanevas[32], E. Katsavounidis[53], W. Katzman[8], K. Kawabe[51], F. Kéfélian[76], D. Keitel[118], J. S. Key[164], S. Khadka[57], F. Y. Khalili[71], I. Khan[17,36], S. Khan[101], E. A. Khazanov[165], N. Khetan[17,18], M. Khursheed[69], N. Kijbunchoo[9], C. Kim[166], G. J. Kim[91], J. C. Kim[167], K. Kim[168], W. Kim[66], W. S. Kim[169], Y.-M. Kim[170], C. Kimball[15], P. J. King[51], M. Kinley-Hanlon[55], R. Kirchhoff[10,11], J. S. Kissel[51], L. Kleybolte[128], S. Klimenko[33], T. D. Knowles[139], E. Knyazev[53], P. Koch[10,11], S. M. Koehlenbeck[10,11], G. Koekoek[40,171], S. Koley[40], M. Kolstein[79], K. Komori[53], V. Kondrashov[1], A. Kontos[62], N. Koper[10,11], M. Korobko[128], W. Z. Korth[1], M. Kovalam[78], D. B. Kozak[1], C. Krämer[10,11], V. Kringel[10,11], N. V. Krishnendu[10,11], A. Królak[172,173], G. Kuehn[10,11], A. Kumar[160], P. Kumar[174], Rahul Kumar[51], Rakesh Kumar[64], K. Kuns[53], S. Kwang[24], B. D. Lackey[89], D. Laghi[19,20], E. Lalande[175], T. L. Lam[104], A. Lamberts[76,176], M. Landry[51], B. B. Lane[53], R. N. Lang[53], J. Lange[132], B. Lantz[57], R. K. Lanza[53], I. La Rosa[38], A. Lartaux-Vollard[31], P. D. Lasky[6], M. Laxen[8], A. Lazzarini[1], C. Lazzaro[60,61], P. Leaci[37,83], S. Leavey[10,11], Y. K. Lecoeuche[51], H. M. Lee[168], H. W. Lee[167], J. Lee[111], K. Lee[57], J. Lehmann[10,11], E. Leon[30], N. Leroy[31], N. Letendre[38], Y. Levin[6], A. Li[1], J. Li[98], K. J. L. Li[104], T. G. F. Li[104], X. Li[77], F. Linde[40,177], S. D. Linker[67], J. N. Linley[55], T. B. Littenberg[178], J. Liu[10,11], X. Liu[24], M. Llorens-Monteagudo[103], R. K. L. Lo[1], A. Lockwood[179], L. T. London[53], A. Longo[180,181], M. Lorenzini[36,102], V. Loriette[182], M. Lormand[8], G. Losurdo[19], J. D. Lough[10,11], C. O. Lousto[132], G. Lovelace[30], M. Lower[43], H. Lück[10,11], D. Lumaca[36,102], A. P. Lundgren[138], Y. Ma[77], R. Macas[101], M. MacInnis[53], D. M. Macleod[101], I. A. O. MacMillan[1], A. Macquet[76], I. Magaña Hernandez[24], F. Magaña-Sandoval[33], C. Magazzù[19], R. M. Magee[140], E. Majorana[37], I. Maksimovic[182], S. Maliakal[1], A. Malik[69], N. Man[76], V. Mandic[47], V. Mangano[37,83], G. L. Mansell[51,53], M. Manske[24], M. Mantovani[32], M. Mapelli[60,61], F. Marchesoni[58,183], F. Marion[38], S. Márka[35], Z. Márka[35], C. Markakis[12], A. S. Markosyan[57], A. Markowitz[1], E. Maros[1], A. Marquina[120], S. Marsat[29], F. Martelli[74,75], I. W. Martin[55], R. M. Martin[39], M. Martinez[79], V. Martinez[23], D. V. Martynov[14], H. Masalehdan[128], K. Mason[53], E. Massera[130], A. Masserot[38], T. J. Massinger[53], M. Masso-Reid[55], S. Mastrogiovanni[29], A. Matas[89], M. Mateu-Lucena[118], F. Matichard[1,53], M. Matiushechkina[10,11], N. Mavalvala[53], E. Maynard[2], J. J. McCann[78], R. McCarthy[51], D. E. McClelland[9], S. McCormick[8], L. McCuller[53], S. C. McGuire[184], C. McIsaac[138], J. McIver[152], D. J. McManus[9], T. McRae[9], S. T. McWilliams[139], D. Meacher[24], G. D. Meadors[6], M. Mehmet[10,11], A. K. Mehta[89], A. Melatos[117], D. A. Melchor[30], G. Mendell[51], A. Menendez-Vazquez[79], R. A. Mercer[24], L. Mereni[131], K. Merfeld[44], E. L. Merilh[51], J. D. Merritt[44], M. Merzougui[76], S. Meshkov[1], C. Messenger[55], C. Messick[185], R. Metzdorff[85], P. M. Meyers[117], F. Meylahn[10,11], A. Mhaske[3], A. Miani[136,137], H. Miao[14], I. Michaloliakos[33], C. Michel[131], H. Middleton[117], L. Milano[5,94], A. L. Miller[33,86], M. Millhouse[117], J. C. Mills[101], E. Milotti[27,186], M. C. Milovich-Goff[67], O. Minazzoli[76,187], Y. Minenkov[36], Ll. M. Mir[79], A. Mishkin[33], C. Mishra[188], T. Mistry[130], S. Mitra[3], V. P. Mitrofanov[71], G. Mitselmakher[33], R. Mittleman[53], G. Mo[53], K. Mogushi[70], S. R. P. Mohapatra[53], S. R. Mohite[24], I. Molina[30], M. Molina-Ruiz[159], M. Mondin[67], M. Montani[74,75], C. J. Moore[14], D. Moraru[51], F. Morawski[65], G. Moreno[51], S. Morisaki[97], B. Mours[189], C. M. Mow-Lowry[14], S. Mozzon[138], F. Muciaccia[37,83], Arunava Mukherjee[55], D. Mukherjee[140], Soma Mukherjee[123], Subroto Mukherjee[64], N. Mukund[10,11], A. Mullavey[8], J. Munch[66], E. A. Muñiz[45], P. G. Murray[55], S. L. Nadji[10,11], A. Nagar[42,190,191], I. Nardecchia[36,102], L. Naticchioni[37], R. K. Nayak[192], B. F. Neil[78], J. Neilson[81,135], G. Nelemans[193], T. J. N. Nelson[8], M. Nery[10,11], A. Neunzert[164], K. Y. Ng[53], S. Ng[66], C. Nguyen[29], P. Nguyen[44], T. Nguyen[53], S. A. Nichols[2], S. Nissanke[40,149], F. Nocera[32], M. Noh[152], C. North[101], D. Nothard[194], L. K. Nuttall[138], J. Oberling[51], B. D. O'Brien[33], J. O'Dell[116], G. Oganesyan[17,18], G. H. Ogin[195], J. J. Oh[169], S. H. Oh[169], F. Ohme[10,11], H. Ohta[97], M. A. Okada[16], C. Olivetto[32], P. Oppermann[10,11], R. J. Oram[8], B. O'Reilly[8], R. G. Ormiston[47], L. F. Ortega[33], R. O'Shaughnessy[132], S. Ossokine[89], C. Osthelder[1],

D. J. Ottaway[66], H. Overmier[8], B. J. Owen[121], A. E. Pace[140], G. Pagano[19,20], M. A. Page[78], G. Pagliaroli[17,18], A. Pai[105], S. A. Pai[69], J. R. Palamos[44], O. Palashov[165], C. Palomba[37], H. Pan[106], P. K. Panda[160], T. H. Pang[40,155], C. Pankow[15], F. Pannarale[37,83], B. C. Pant[69], F. Paoletti[19], A. Paoli[32], A. Paolone[37,196], W. Parker[8,184], D. Pascucci[40], A. Pasqualetti[32], R. Passaquieti[19,20], D. Passuello[19], M. Patel[7], B. Patricelli[19,20], E. Payne[6], T. C. Pechsiri[33], M. Pedraza[1], M. Pegoraro[61], A. Pele[8], S. Penn[197], A. Perego[136,137], C. J. Perez[51], C. Périgois[38], A. Perreca[136,137], S. Perriès[110], J. Petermann[128], D. Petterson[1], H. P. Pfeiffer[89], K. A. Pham[47], K. S. Phukon[3,40,177], O. J. Piccinni[37,83], M. Pichot[76], M. Piendibene[19,20], F. Piergiovanni[74,75], L. Pierini[37,83], V. Pierro[81,135], G. Pillant[32], F. Pilo[19], L. Pinard[131], I. M. Pinto[81,135,190], K. Piotrzkowski[86], M. Pirello[51], M. Pitkin[198], E. Placidi[83], W. Plastino[180,181], C. Pluchar[115], R. Poggiani[19,20], E. Polini[38], D. Y. T. Pong[104], S. Ponrathnam[3], P. Popolizio[32], E. K. Porter[29], A. Poverman[62], J. Powell[43], M. Pracchia[38], A. K. Prajapati[64], K. Prasai[57], R. Prasanna[160], G. Pratten[14], T. Prestegard[24], M. Principe[81,135,190], G. A. Prodi[137,199], L. Prokhorov[14], P. Prosposito[36,102], A. Puecher[40,155], M. Punturo[58], F. Puosi[19,20], P. Puppo[37], M. Pürrer[89], H. Qi[101], V. Quetschke[123], P. J. Quinonez[28], R. Quitzow-James[70], F. J. Raab[51], G. Raaijmakers[40,149], H. Radkins[51], N. Radulesco[76], P. Raffai[126], H. Rafferty[200], S. X. Rail[175], S. Raja[69], C. Rajan[69], B. Rajbhandari[121], M. Rakhmanov[123], K. E. Ramirez[123], T. D. Ramirez[30], A. Ramos-Buades[118], J. Rana[140], K. Rao[15], P. Rapagnani[37,83], U. D. Rapol[201], B. Ratto[28], V. Raymond[101], M. Razzano[19,20], J. Read[30], D. J. Reardon[43], T. Regimbau[38], L. Rei[68], S. Reid[25], D. H. Reitze[1,33], P. Rettegno[42,202], F. Ricci[37,83], C. J. Richardson[28], J. W. Richardson[1], L. Richardson[115], P. M. Ricker[22], G. Riemenschneider[42,202], K. Riles[156], M. Rizzo[15], N. A. Robertson[1,55], F. Robinet[31], A. Rocchi[36], J. A. Rocha[30], S. Rodriguez[30], R. D. Rodriguez-Soto[28], L. Rolland[38], J. G. Rollins[1], V. J. Roma[44], M. Romanelli[84], R. Romano[4,5], C. L. Romel[51], A. Romero[79], I. M. Romero-Shaw[6], J. H. Romie[8], S. Ronchini[17,18], C. A. Rose[24], D. Rose[30], K. Rose[194], D. Rosińska[87], S. G. Rosofsky[22], M. P. Ross[179], S. Rowan[55], S. J. Rowlinson[14], Santosh Roy[3], Soumen Roy[203], P. Ruggi[32], K. Ryan[51], S. Sachdev[140], T. Sadecki[51], J. Sadiq[132], M. Sakellariadou[113], O. S. Salafia[48,49,50], L. Salconi[32], M. Saleem[34], A. Samajdar[40,155], E. J. Sanchez[1], J. H. Sanchez[30], L. E. Sanchez[1], N. Sanchis-Gual[204], J. R. Sanders[205], K. A. Santiago[39], E. Santos[76], T. R. Saravanan[3], N. Sarin[6], B. Sassolas[131], O. Sauter[38], R. L. Savage[51], V. Savant[3], D. Sawant[105], S. Sayah[131], D. Schaetzl[1], P. Schale[44], M. Scheel[77], J. Scheuer[15], A. Schindler-Tyka[33], P. Schmidt[14], R. Schnabel[128], R. M. S. Schofield[44], A. Schönbeck[128], E. Schreiber[10,11], B. W. Schulte[10,11], B. F. Schutz[10,101], O. Schwarm[195], E. Schwartz[101], J. Scott[55], S. M. Scott[9], M. Seglar-Arroyo[38], E. Seidel[22], D. Sellers[8], A. S. Sengupta[203], N. Sennett[89], D. Sentenac[32], V. Sequino[5,94], A. Sergeev[165], Y. Setyawati[10,11], T. Shaffer[51], M. S. Shahriar[15], S. Sharifi[2], A. Sharma[17,18], P. Sharma[69], P. Shawhan[90], H. Shen[22], M. Shikauchi[97], R. Shink[175], D. H. Shoemaker[53], D. M. Shoemaker[91], K. Shukla[159], S. ShyamSundar[69], M. Sieniawska[65], D. Sigg[51], L. P. Singer[95], D. Singh[140], N. Singh[87], A. Singha[127], A. Singhal[17,37], A. M. Sintes[118], V. Sipala[99,100], V. Skliris[101], B. J. J. Slagmolen[9], T. J. Slaven-Blair[78], J. Smetana[14], J. R. Smith[30], R. J. E. Smith[6], S. N. Somala[206], E. J. Son[169], S. Soni[2], B. Sorazu[55], V. Sordini[110], F. Sorrentino[68], N. Sorrentino[19,20], R. Soulard[76], T. Souradeep[3,201], E. Sowell[121], A. P. Spencer[55], M. Spera[15,60,61], A. K. Srivastava[64], V. Srivastava[45], K. Staats[15], C. Stachie[76], D. A. Steer[29], M. Steinke[10,11], J. Steinlechner[55,127], S. Steinlechner[127], D. Steinmeyer[10,11], G. Stolle-McAllister[194], D. J. Stops[14], M. Stover[194], K. A. Strain[55], G. Stratta[75,207], A. Strunk[51], R. Sturani[208], A. L. Stuver[92], J. Südbeck[128], S. Sudhagar[3], V. Sudhir[53], T. Z. Summerscales[209], H. Sun[78], L. Sun[1], S. Sunil[64], A. Sur[65], J. Suresh[97], P. J. Sutton[101], B. L. Swinkels[40], M. J. Szczepańczyk[33], M. Tacca[40], S. C. Tait[55], C. Talbot[6], A. J. Tanasijczuk[86], D. B. Tanner[33], D. Tao[1], A. Tapia[30], E. N. Tapia San Martin[40], J. D. Tasson[158], R. Taylor[1], R. Tenorio[118], L. Terkowski[128], M. P. Thirugnanasambandam[3], M. Thomas[8], P. Thomas[51], J. E. Thompson[101], S. R. Thondapu[69], K. A. Thorne[8], E. Thrane[6], Shubhanshu Tiwari[82], Srishti Tiwari[153], V. Tiwari[101], K. Toland[55], A. E. Tolley[138], M. Tonelli[19,20], Z. Tornasi[55], A. Torres-Forné[89], C. I. Torrie[1], I. Tosta e Melo[99,100], D. Töyrä[9], A. T. Tran[124], A. Trapananti[58,183], F. Travasso[58,183], G. Traylor[8], M. C. Tringali[87], A. Tripathee[156], A. Trovato[29], R. J. Trudeau[1], D. S. Tsai[106], K. W. Tsang[40,155,210], M. Tse[53], R. Tso[77], L. Tsukada[97], D. Tsuna[97], T. Tsutsui[97], M. Turconi[76], A. S. Ubhi[14], R. P. Udall[91], K. Ueno[97], D. Ugolini[200], C. S. Unnikrishnan[153], A. L. Urban[2], S. A. Usman[108], A. C. Utina[127], H. Vahlbruch[10,11], G. Vajente[1], A. Vajpeyi[6], G. Valdes[2], M. Valentini[136,137], V. Valsan[24], N. van Bakel[40], M. van Beuzekom[40], J. F. J. van den Brand[40,88,171], C. Van Den Broeck[40,155], D. C. Vander-Hyde[45], L. van der Schaaf[40], J. V. van Heijningen[78], M. Vardaro[40,177], A. F. Vargas[117], V. Varma[77], S. Vass[1], M. Vasúth[56], A. Vecchio[14], G. Vedovato[61], J. Veitch[55], P. J. Veitch[66], K. Venkateswara[179], J. Venneberg[10,11], G. Venugopalan[1], D. Verkindt[38], Y. Verma[69], D. Veske[35], F. Vetrano[74], A. Viceré[74,75], A. D. Viets[211], V. Villa-Ortega[129], J.-Y. Vinet[76], S. Vitale[53], T. Vo[45], H. Vocca[58,59], C. Vorvick[51], S. P. Vyatchanin[71], A. R. Wade[9], L. E. Wade[194], M. Wade[194], R. C. Walet[40], M. Walker[7], G. S. Wallace[25], L. Wallace[1], S. Walsh[24], J. Z. Wang[156], S. Wang[22], W. H. Wang[123], Y. F. Wang[104], R. L. Ward[9], J. Warner[51], M. Was[38], N. Y. Washington[1], J. Watchi[119], B. Weaver[51], L. Wei[10,11], M. Weinert[10,11], A. J. Weinstein[1], R. Weiss[53], F. Wellmann[10,11], L. Wen[78], P. Weßels[10,11], J. W. Westhouse[28], K. Wette[9], J. T. Whelan[132], D. D. White[30], L. V. White[45], B. F. Whiting[33], C. Whittle[53], D. M. Wilken[10,11], D. Williams[55], M. J. Williams[55], A. R. Williamson[138], J. L. Willis[1], B. Willke[10,11], D. J. Wilson[115], M. H. Wimmer[10,11], W. Winkler[10,11], C. C. Wipf[1], G. Woan[55], J. Woehler[10,11], J. K. Wofford[132], I. C. F. Wong[104], J. Wrangel[10,11], J. L. Wright[55], D. S. Wu[10,11], D. M. Wysocki[132], L. Xiao[1], H. Yamamoto[1], L. Yang[142], Y. Yang[33], Z. Yang[47], M. J. Yap[9], D. W. Yeeles[101], A. Yoon[7], Hang Yu[77], Haocun Yu[53], S. H. R. Yuen[104], A. Zadrożny[173], M. Zanolin[28], T. Zelenova[32], J.-P. Zendri[61], M. Zevin[15], J. Zhang[78], L. Zhang[1], R. Zhang[33], T. Zhang[14], C. Zhao[78], G. Zhao[119], M. Zhou[15], Z. Zhou[15], X. J. Zhu[6], M. E. Zucker[1,53], J. Zweizig[1]

The LIGO Scientific Collaboration and the Virgo Collaboration,

M. J. Keith[212], A. G. Lyne[212], J. Palfreyman[213], B. Shaw[212], B. W. Stappers[212], and P. Weltevrede[212]

[1] LIGO, California Institute of Technology, Pasadena, CA 91125, USA

[2] Louisiana State University, Baton Rouge, LA 70803, USA

[3] Inter-University Centre for Astronomy and Astrophysics, Pune 411007, India
[4] Dipartimento di Farmacia, Università di Salerno, I-84084 Fisciano, Salerno, Italy
[5] INFN, Sezione di Napoli, Complesso Universitario di Monte S.Angelo, I-80126 Napoli, Italy
[6] OzGrav, School of Physics & Astronomy, Monash University, Clayton 3800, Victoria, Australia
[7] Christopher Newport University, Newport News, VA 23606, USA
[8] LIGO Livingston Observatory, Livingston, LA 70754, USA
[9] OzGrav, Australian National University, Canberra, Australian Capital Territory 0200, Australia
[10] Max Planck Institute for Gravitational Physics (Albert Einstein Institute), D-30167 Hannover, Germany
[11] Leibniz Universität Hannover, D-30167 Hannover, Germany
[12] University of Cambridge, Cambridge CB2 1TN, UK
[13] Theoretisch-Physikalisches Institut, Friedrich-Schiller-Universität Jena, D-07743 Jena, Germany
[14] University of Birmingham, Birmingham B15 2TT, UK
[15] Center for Interdisciplinary Exploration & Research in Astrophysics (CIERA), Northwestern University, Evanston, IL 60208, USA
[16] Instituto Nacional de Pesquisas Espaciais, 12227-010 São José dos Campos, São Paulo, Brazil
[17] Gran Sasso Science Institute (GSSI), I-67100 L'Aquila, Italy
[18] INFN, Laboratori Nazionali del Gran Sasso, I-67100 Assergi, Italy
[19] INFN, Sezione di Pisa, I-56127 Pisa, Italy
[20] Università di Pisa, I-56127 Pisa, Italy
[21] International Centre for Theoretical Sciences, Tata Institute of Fundamental Research, Bengaluru 560089, India
[22] NCSA, University of Illinois at Urbana-Champaign, Urbana, IL 61801, USA
[23] Université de Lyon, Université Claude Bernard Lyon 1, CNRS, Institut Lumière Matière, F-69622 Villeurbanne, France
[24] University of Wisconsin-Milwaukee, Milwaukee, WI 53201, USA
[25] SUPA, University of Strathclyde, Glasgow G1 1XQ, UK
[26] Dipartimento di Matematica e Informatica, Università di Udine, I-33100 Udine, Italy
[27] INFN, Sezione di Trieste, I-34127 Trieste, Italy
[28] Embry-Riddle Aeronautical University, Prescott, AZ 86301, USA
[29] Université de Paris, CNRS, Astroparticule et Cosmologie, F-75013 Paris, France
[30] California State University Fullerton, Fullerton, CA 92831, USA
[31] Université Paris-Saclay, CNRS/IN2P3, IJCLab, F-91405 Orsay, France
[32] European Gravitational Observatory (EGO), I-56021 Cascina, Pisa, Italy
[33] University of Florida, Gainesville, FL 32611, USA
[34] Chennai Mathematical Institute, Chennai 603103, India
[35] Columbia University, New York, NY 10027, USA
[36] INFN, Sezione di Roma Tor Vergata, I-00133 Roma, Italy
[37] INFN, Sezione di Roma, I-00185 Roma, Italy
[38] Laboratoire d'Annecy de Physique des Particules (LAPP), Univ. Grenoble Alpes, Université Savoie Mont Blanc, CNRS/IN2P3, F-74941 Annecy, France
[39] Montclair State University, Montclair, NJ 07043, USA
[40] Nikhef, Science Park 105, 1098 XG Amsterdam, Netherlands
[41] Korea Institute of Science and Technology Information, Daejeon 34141, Republic of Korea
[42] INFN Sezione di Torino, I-10125 Torino, Italy
[43] OzGrav, Swinburne University of Technology, Hawthorn VIC 3122, Australia
[44] University of Oregon, Eugene, OR 97403, USA
[45] Syracuse University, Syracuse, NY 13244, USA
[46] Université de Liège, B-4000 Liège, Belgium
[47] University of Minnesota, Minneapolis, MN 55455, USA
[48] Università degli Studi di Milano-Bicocca, I-20126 Milano, Italy
[49] INFN, Sezione di Milano-Bicocca, I-20126 Milano, Italy
[50] INAF, Osservatorio Astronomico di Brera sede di Merate, I-23807 Merate, Lecco, Italy
[51] LIGO Hanford Observatory, Richland, WA 99352, USA
[52] Institut de Ciències del Cosmos, Universitat de Barcelona, C/ Martí i Franquès 1, Barcelona, E-08028, Spain
[53] LIGO, Massachusetts Institute of Technology, Cambridge, MA 02139, USA
[54] Dipartimento di Medicina, Chirurgia e Odontoiatria "Scuola Medica Salernitana," Università di Salerno, I-84081 Baronissi, Salerno, Italy
[55] SUPA, University of Glasgow, Glasgow G12 8QQ, UK
[56] Wigner RCP, RMKI, H-1121 Budapest, Konkoly Thege Miklós út 29-33, Hungary
[57] Stanford University, Stanford, CA 94305, USA
[58] INFN, Sezione di Perugia, I-06123 Perugia, Italy
[59] Università di Perugia, I-06123 Perugia, Italy
[60] Università di Padova, Dipartimento di Fisica e Astronomia, I-35131 Padova, Italy
[61] INFN, Sezione di Padova, I-35131 Padova, Italy
[62] Bard College, 30 Campus Rd, Annandale-On-Hudson, NY 12504, USA
[63] Montana State University, Bozeman, MT 59717, USA
[64] Institute for Plasma Research, Bhat, Gandhinagar 382428, India
[65] Nicolaus Copernicus Astronomical Center, Polish Academy of Sciences, 00-716, Warsaw, Poland
[66] OzGrav, University of Adelaide, Adelaide, South Australia 5005, Australia
[67] California State University, Los Angeles, 5151 State University Drive, Los Angeles, CA 90032, USA
[68] INFN, Sezione di Genova, I-16146 Genova, Italy
[69] RRCAT, Indore, Madhya Pradesh 452013, India
[70] Missouri University of Science and Technology, Rolla, MO 65409, USA
[71] Faculty of Physics, Lomonosov Moscow State University, Moscow 119991, Russia
[72] SUPA, University of the West of Scotland, Paisley PA1 2BE, UK
[73] Bar-Ilan University, Ramat Gan, 5290002, Israel
[74] Università degli Studi di Urbino "Carlo Bo," I-61029 Urbino, Italy
[75] INFN, Sezione di Firenze, I-50019 Sesto Fiorentino, Firenze, Italy
[76] Artemis, Université Côte d'Azur, Observatoire Côte d'Azur, CNRS, F-06304 Nice, France
[77] Caltech CaRT, Pasadena, CA 91125, USA
[78] OzGrav, University of Western Australia, Crawley, Western Australia 6009, Australia

[79] Institut de Física d'Altes Energies (IFAE), Barcelona Institute of Science and Technology, and ICREA, E-08193 Barcelona, Spain
[80] Dipartimento di Fisica "E.R. Caianiello," Università di Salerno, I-84084 Fisciano, Salerno, Italy
[81] INFN, Sezione di Napoli, Gruppo Collegato di Salerno, Complesso Universitario di Monte S. Angelo, I-80126 Napoli, Italy
[82] Physik-Institut, University of Zurich, Winterthurerstrasse 190, 8057 Zurich, Switzerland
[83] Università di Roma "La Sapienza," I-00185 Roma, Italy
[84] Univ Rennes, CNRS, Institut FOTON—UMR6082, F-3500 Rennes, France
[85] Laboratoire Kastler Brossel, Sorbonne Université, CNRS, ENS-Université PSL, Collège de France, F-75005 Paris, France
[86] Université catholique de Louvain, B-1348 Louvain-la-Neuve, Belgium
[87] Astronomical Observatory Warsaw University, 00-478 Warsaw, Poland
[88] VU University Amsterdam, 1081 HV Amsterdam, Netherlands
[89] Max Planck Institute for Gravitational Physics (Albert Einstein Institute), D-14476 Potsdam-Golm, Germany
[90] University of Maryland, College Park, MD 20742, USA
[91] School of Physics, Georgia Institute of Technology, Atlanta, GA 30332, USA
[92] Villanova University, 800 Lancaster Avenue, Villanova, PA 19085, USA
[93] Center for Computational Astrophysics, Flatiron Institute, New York, NY 10010, USA
[94] Università di Napoli "Federico II," Complesso Universitario di Monte S.Angelo, I-80126 Napoli, Italy
[95] NASA Goddard Space Flight Center, Greenbelt, MD 20771, USA
[96] Dipartimento di Fisica, Università degli Studi di Genova, I-16146 Genova, Italy
[97] RESCEU, University of Tokyo, Tokyo, 113-0033, Japan
[98] Tsinghua University, Beijing 100084, People's Republic of China
[99] Università degli Studi di Sassari, I-07100 Sassari, Italy
[100] INFN, Laboratori Nazionali del Sud, I-95125 Catania, Italy
[101] Gravity Exploration Institute, Cardiff University, Cardiff CF24 3AA, UK
[102] Università di Roma Tor Vergata, I-00133 Roma, Italy
[103] Departamento de Astronomía y Astrofísica, Universitat de València, E-46100 Burjassot, València, Spain
[104] The Chinese University of Hong Kong, Shatin, NT, Hong Kong
[105] Indian Institute of Technology Bombay, Powai, Mumbai 400 076, India
[106] National Tsing Hua University, Hsinchu City, 30013 Taiwan, Republic of China
[107] Charles Sturt University, Wagga Wagga, New South Wales 2678, Australia
[108] University of Chicago, Chicago, IL 60637, USA
[109] Dipartimento di Ingegneria Industriale (DIIN), Università di Salerno, I-84084 Fisciano, Salerno, Italy
[110] Institut de Physique des 2 Infinis de Lyon, CNRS/IN2P3, Université de Lyon, Université Claude Bernard Lyon 1, F-69622 Villeurbanne, France
[111] Seoul National University, Seoul 08826, Republic of Korea
[112] Pusan National University, Busan 46241, Republic of Korea
[113] King's College London, University of London, London WC2R 2LS, UK
[114] INAF, Osservatorio Astronomico di Padova, I-35122 Padova, Italy
[115] University of Arizona, Tucson, AZ 85721, USA
[116] Rutherford Appleton Laboratory, Didcot OX11 0DE, UK
[117] OzGrav, University of Melbourne, Parkville, Victoria 3010, Australia
[118] Universitat de les Illes Balears, IAC3—IEEC, E-07122 Palma de Mallorca, Spain
[119] Université Libre de Bruxelles, Brussels B-1050, Belgium
[120] Departamento de Matemáticas, Universitat de València, E-46100 Burjassot, València, Spain
[121] Texas Tech University, Lubbock, TX 79409, USA
[122] University of Rhode Island, Kingston, RI 02881, USA
[123] The University of Texas Rio Grande Valley, Brownsville, TX 78520, USA
[124] Bellevue College, Bellevue, WA 98007, USA
[125] Scuola Normale Superiore, Piazza dei Cavalieri, 7, I-56126 Pisa, Italy
[126] MTA-ELTE Astrophysics Research Group, Institute of Physics, Eötvös University, Budapest 1117, Hungary
[127] Maastricht University, 6200 MD, Maastricht, Netherlands
[128] Universität Hamburg, D-22761 Hamburg, Germany
[129] IGFAE, Campus Sur, Universidade de Santiago de Compostela, E-15782, Spain
[130] The University of Sheffield, Sheffield S10 2TN, UK
[131] Laboratoire des Matériaux Avancés (LMA), Institut de Physique des 2 Infinis de Lyon, CNRS/IN2P3, Université de Lyon, F-69622 Villeurbanne, France
[132] Rochester Institute of Technology, Rochester, NY 14623, USA
[133] Dipartimento di Scienze Matematiche, Fisiche e Informatiche, Università di Parma, I-43124 Parma, Italy
[134] INFN, Sezione di Milano Bicocca, Gruppo Collegato di Parma, I-43124 Parma, Italy
[135] Dipartimento di Ingegneria, Università del Sannio, I-82100 Benevento, Italy
[136] Università di Trento, Dipartimento di Fisica, I-38123 Povo, Trento, Italy
[137] INFN, Trento Institute for Fundamental Physics and Applications, I-38123 Povo, Trento, Italy
[138] University of Portsmouth, Portsmouth, PO1 3FX, UK
[139] West Virginia University, Morgantown, WV 26506, USA
[140] The Pennsylvania State University, University Park, PA 16802, USA
[141] Stony Brook University, Stony Brook, NY 11794, USA
[142] Colorado State University, Fort Collins, CO 80523, USA
[143] Institute for Nuclear Research, Hungarian Academy of Sciences, Bem t'er 18/c, H-4026 Debrecen, Hungary
[144] CNR-SPIN, c/o Università di Salerno, I-84084 Fisciano, Salerno, Italy
[145] Scuola di Ingegneria, Università della Basilicata, I-85100 Potenza, Italy
[146] National Astronomical Observatory of Japan, 2-21-1 Osawa, Mitaka, Tokyo 181-8588, Japan
[147] Observatori Astronòmic, Universitat de València, E-46980 Paterna, València, Spain
[148] University of Szeged, Dóm tér 9, Szeged 6720, Hungary
[149] GRAPPA, Anton Pannekoek Institute for Astronomy and Institute for High-Energy Physics, University of Amsterdam, Science Park 904, 1098 XH Amsterdam, Netherlands
[150] Delta Institute for Theoretical Physics, Science Park 904, 1090 GL Amsterdam, Netherlands
[151] Lorentz Institute, Leiden University, Niels Bohrweg 2, 2333 CA Leiden, Netherlands
[152] University of British Columbia, Vancouver, BC V6T 1Z4, Canada
[153] Tata Institute of Fundamental Research, Mumbai 400005, India

[154] INAF, Osservatorio Astronomico di Capodimonte, I-80131 Napoli, Italy
[155] Department of Physics, Utrecht University, Princetonplein 1, 3584 CC Utrecht, Netherlands
[156] University of Michigan, Ann Arbor, MI 48109, USA
[157] American University, Washington, DC 20016, USA
[158] Carleton College, Northfield, MN 55057, USA
[159] University of California, Berkeley, CA 94720, USA
[160] Directorate of Construction, Services & Estate Management, Mumbai 400094, India
[161] Universiteit Antwerpen, Prinsstraat 13, B-2000 Antwerpen, Belgium
[162] University of Bialystok, 15-424 Bialystok, Poland
[163] University of Southampton, Southampton SO17 1BJ, UK
[164] University of Washington Bothell, Bothell, WA 98011, USA
[165] Institute of Applied Physics, Nizhny Novgorod, 603950, Russia
[166] Ewha Womans University, Seoul 03760, Republic of Korea
[167] Inje University Gimhae, South Gyeongsang 50834, Republic of Korea
[168] Korea Astronomy and Space Science Institute, Daejeon 34055, Republic of Korea
[169] National Institute for Mathematical Sciences, Daejeon 34047, Republic of Korea
[170] Ulsan National Institute of Science and Technology, Ulsan 44919, Republic of Korea
[171] Maastricht University, P.O. Box 616, 6200 MD Maastricht, Netherlands
[172] Institute of Mathematics, Polish Academy of Sciences, 00656 Warsaw, Poland
[173] National Center for Nuclear Research, 05-400 Swierk-Otwock, Poland
[174] Cornell University, Ithaca, NY 14850, USA
[175] Université de Montréal/Polytechnique, Montreal, Quebec H3T 1J4, Canada
[176] Laboratoire Lagrange, Université Côte d'Azur, Observatoire Côte d'Azur, CNRS, F-06304 Nice, France
[177] Institute for High-Energy Physics, University of Amsterdam, Science Park 904, 1098 XH Amsterdam, Netherlands
[178] NASA Marshall Space Flight Center, Huntsville, AL 35811, USA
[179] University of Washington, Seattle, WA 98195, USA
[180] Dipartimento di Matematica e Fisica, Università degli Studi Roma Tre, I-00146 Roma, Italy
[181] INFN, Sezione di Roma Tre, I-00146 Roma, Italy
[182] ESPCI, CNRS, F-75005 Paris, France
[183] Università di Camerino, Dipartimento di Fisica, I-62032 Camerino, Italy
[184] Southern University and A&M College, Baton Rouge, LA 70813, USA
[185] Department of Physics, University of Texas, Austin, TX 78712, USA
[186] Dipartimento di Fisica, Università di Trieste, I-34127 Trieste, Italy
[187] Centre Scientifique de Monaco, 8 quai Antoine Ier, MC-98000, Monaco
[188] Indian Institute of Technology Madras, Chennai 600036, India
[189] Institut Pluridisciplinaire Hubert CURIEN, 23 rue du loess—BP28 F-67037 Strasbourg cedex 2, France
[190] Museo Storico della Fisica e Centro Studi e Ricerche "Enrico Fermi," I-00184 Roma, Italy
[191] Institut des Hautes Etudes Scientifiques, F-91440 Bures-sur-Yvette, France
[192] Indian Institute of Science Education and Research, Kolkata, Mohanpur, West Bengal 741252, India
[193] Department of Astrophysics/IMAPP, Radboud University Nijmegen, P.O. Box 9010, 6500 GL Nijmegen, Netherlands
[194] Kenyon College, Gambier, OH 43022, USA
[195] Whitman College, 345 Boyer Avenue, Walla Walla, WA 99362, USA
[196] Consiglio Nazionale delle Ricerche—Istituto dei Sistemi Complessi, Piazzale Aldo Moro 5, I-00185 Roma, Italy
[197] Hobart and William Smith Colleges, Geneva, NY 14456, USA
[198] Lancaster University, Lancaster LA1 4YW, UK
[199] Università di Trento, Dipartimento di Matematica, I-38123 Povo, Trento, Italy
[200] Trinity University, San Antonio, TX 78212, USA
[201] Indian Institute of Science Education and Research, Pune, Maharashtra 411008, India
[202] Dipartimento di Fisica, Università degli Studi di Torino, I-10125 Torino, Italy
[203] Indian Institute of Technology, Palaj, Gandhinagar, Gujarat 382355, India
[204] Centro de Astrofísica e Gravitação (CENTRA), Departamento de Física, Instituto Superior Técnico, Universidade de Lisboa, 1049-001 Lisboa, Portugal
[205] Marquette University, 11420 W. Clybourn Street, Milwaukee, WI 53233, USA
[206] Indian Institute of Technology Hyderabad, Sangareddy, Khandi, Telangana 502285, India
[207] INAF, Osservatorio di Astrofisica e Scienza dello Spazio, I-40129 Bologna, Italy
[208] International Institute of Physics, Universidade Federal do Rio Grande do Norte, Natal RN 59078-970, Brazil
[209] Andrews University, Berrien Springs, MI 49104, USA
[210] Van Swinderen Institute for Particle Physics and Gravity, University of Groningen, Nijenborgh 4, 9747 AG Groningen, Netherlands
[211] Concordia University Wisconsin, Mequon, WI 53097, USA
[212] Jodrell Bank Centre for Astrophysics, School of Physics and Astronomy, University of Manchester, Manchester, M13 9PL, UK
[213] Department of Physical Sciences, University of Tasmania, Private Bag 37, Hobart, Tasmania 7001, Australia; lsc-spokesperson@ligo.org, virgo-spokesperson@ego-gw.it

Received 2020 July 28; revised 2020 September 4; accepted 2020 September 5; published 2020 October 12

Abstract

We present a search for continuous gravitational waves from five radio pulsars, comprising three recycled pulsars (PSR J0437−4715, PSR J0711−6830, and PSR J0737−3039A) and two young pulsars: the Crab pulsar (J0534+2200) and the Vela pulsar (J0835−4510). We use data from the third observing run of Advanced LIGO and Virgo combined with data from their first and second observing runs. For the first time, we are able to match (for PSR J0437−4715) or surpass (for PSR J0711−6830) the indirect limits on gravitational-wave emission from recycled pulsars inferred from their observed spin-downs, and constrain their equatorial ellipticities to be less than 10^{-8}. For each of the five pulsars, we perform targeted searches that assume a tight coupling between the gravitational-wave and electromagnetic signal phase evolution. We also present constraints on PSR J0711−6830, the Crab pulsar, and the Vela pulsar from a search that relaxes this assumption, allowing the

gravitational-wave signal to vary from the electromagnetic expectation within a narrow band of frequencies and frequency derivatives.

Unified Astronomy Thesaurus concepts: Gravitational waves (678); Neutron stars (1108); Pulsars (1306); Gravitational wave sources (677)

Supporting material: machine-readable table

1. Introduction

The field of gravitational-wave astronomy is now firmly established, with the detection of multiple compact binary coalescences by the LIGO and Virgo observatories. These discoveries have included multiple black hole–black hole coalescences (Abbott et al. 2019c) and binary neutron star coalescences (Abbott et al. 2017a, 2020b). Resulting studies have included tests of strong-field general relativity (Abbott et al. 2019d), measurement of the Hubble parameter (Abbott et al. 2017b, 2019e; Fishbach et al. 2019), confirmation of the association between binary neutron star coalescence and short gamma-ray bursts (Abbott et al. 2017c), and information on the pressure–density relation for ultra-high-density matter (Abbott et al. 2018a).

Other types of gravitational-wave sources, however, remain to be detected, including *continuous wave* (CW) sources. CWs have a relatively simple structure, consisting of just one or two harmonic components, whose amplitudes and frequencies change slowly on the year-long timescales of observations. The prime candidates for producing such CW signals are spinning neutron stars that have non-axisymmetric distortions, caused either by a solid deformation, probably sourced through some combination of elastic and magnetic stresses, or by the excitation of fluid modes of oscillation also referred to as *r-modes* (Alford & Schwenzer 2015). The astrophysical payoff in making a detection would be considerable, shedding light on the structure of the star. Moreover a CW detection would allow further tests of general relativity, such as constraining nonstandard gravitational-wave polarizations (Isi et al. 2017). A recent review of the astrophysics of CW sources is given in Glampedakis & Gualtieri (2018).

1.1. Continuous Wave Searches

CW searches can be divided into three main types. *Targeted searches* look for signals from known pulsars whose rotational phase is accurately determined from electromagnetic observations, considerably simplifying the search. *Directed searches* look for signals from small sky areas, such as supernova remnants, where a neutron star is believed to reside, but for which no timing solution exists, so that a wide range of rotational parameters needs to be searched over. *All-sky* searches look for signals over all sky directions and also over a wide range of rotational parameters. Many searches of these three types have already been carried out, using LIGO and Virgo data. For recent examples, see Abbott et al. (2019a, 2019f, 2019g). No detections have been made, and consequently upper limits have been set on the strengths of such signals.

In this paper we report new results of targeted searches for CW signals from five pulsars, using the most recent LIGO and Virgo data sets. Specifically, we use data from the first and second observing runs (O1 and O2), together with data from the first half of the third observing run (O3a), allowing us to set improved upper limits compared to other recent searches (e.g., Abbott et al. 2019a).

It is possible to carry out such searches for many more (several hundred) known pulsars (Abbott et al. 2019a). We report results here for pulsars of particular interest. Specifically, we target three older, recycled pulsars, two of which are millisecond pulsars and one of which is only mildly recycled, that are believed to have undergone periods of accretion, and two very young pulsars: Crab and Vela. We search for the older pulsars, and particularly the recycled pulsars, because the signal amplitude is proportional to the square of the frequency, and therefore only small distortions are necessary to make a detection possible (see Equation (4)). The young pulsars are interesting because their rapid spin-down means that only a small fraction of their spin-down energy need go into the gravitational-wave channel for a detection to be possible. Here we obtain direct gravitational-wave observational limits that are at or below the spin-down limits for two of the recycled pulsars. This is the first time the spin-down limit has been equaled or surpassed for a recycled pulsar. As such, this represents a significant milestone for gravitational-wave astronomy.

The structure of this paper is as follows. In Section 1.2 we describe the signal models we used. In Section 2 we discuss the analysis methods used in the searches. In Section 3 we describe both the gravitational-wave data we used, and also the radio pulsar data that was used to produce the timing solutions on which the gravitational-wave searches were based. In Section 4 we describe our results, which are then discussed in Section 5. Finally, in Section 6, we draw some conclusions.

1.2. Signal Models

We will assume gravitational-wave emission that is tied closely to the rotational phase of the star. In the simplest case of a triaxial star spinning steadily about a principal moment-of-inertia axis, the gravitational-wave emission is at exactly twice the star's spin frequency.

There are several mechanisms, however, that can produce slightly different signals. Free precession of the star can produce a small frequency offset between the gravitational-wave and (twice) the spin frequency, and also produce a lower harmonic, at or close to the spin frequency (Zimmermann & Szedenits 1979; Jones & Andersson 2002). In most cases, free precession would modulate the observed radio pulsar frequency, a phenomenon not commonly observed in the pulsar population. However, as noted by Jones (2010), the presence of a superfluid component within the star with a spin axis misaligned from that of the main rotation can produce this dual-harmonic emission, while leaving no imprint on the radio emission. Another possibility is that the dominant gravitational-wave emission is produced by a solid core (Glendenning 1996; Owen 2005) whose spin frequency is slightly greater than that of the crust, again leading to a small mismatch between the gravitational and (twice) the radio pulsar frequency; see Abbott et al. (2008).

With these considerations in mind, we follow previous CW analyses and carry out three different sorts of searches within

this paper. The simplest search assumes a single gravitational-wave component, at exactly twice the observed spin frequency, as deduced from radio pulsar observations. We carry out "dual-harmonic searches," allowing for emission at both one and two times the spin frequency. And we also carry out searches allowing for a small mismatch between the electromagnetic and gravitational signal frequencies, so-called "narrowband" searches.

The basic form of the waveform used in dual-harmonic searches is described in detail in Jones (2015), and used to perform searches in Pitkin et al. (2015), and Abbott et al. (2017d, 2019a). We refer the reader to these papers, and in particular Section 1.1 and Appendix A of Abbott et al. (2017d). We reproduce the main results here for completeness.

If we denote the signals at one and two times the spin frequency as $h_{21}(t)$ and $h_{22}(t)$, respectively, we have

$$h_{21} = -\frac{C_{21}}{2}[F_+^D(\alpha, \delta, \psi; t)\sin\iota\cos\iota\cos(\Phi(t) + \Phi_{21}^C) + F_\times^D(\alpha, \delta, \psi; t)\sin\iota\sin(\Phi(t) + \Phi_{21}^C)], \quad (1)$$

$$h_{22} = -C_{22}[F_+^D(\alpha, \delta, \psi; t)(1 + \cos^2\iota)\cos(2\Phi(t) + \Phi_{22}^C) + 2F_\times^D(\alpha, \delta, \psi; t)\cos\iota\sin(2\Phi(t) + \Phi_{22}^C)]. \quad (2)$$

In these equations, C_{21} and C_{22} are dimensionless constants that give the amplitudes of the components. The angles (α, δ) are the R.A. and decl. of the source, while the angles (ι, ψ) specify the orientation of the star's spin axis relative to the observer. The quantities Φ_{21}^C, Φ_{22}^C are phase angles. The functions F_+^D and $F_\times^D$, known as the antenna or beam functions, describe how the two polarization components of the signal project onto the detector (see, e.g., Jaranowski et al. 1998). The quantity $\Phi(t)$ is the rotational phase of the source.

The special and familiar case of single harmonic emission from a steadily spinning triaxial star is obtained by setting $C_{21} = 0$, leaving only the higher-frequency component. In this case, the amplitude is more conventionally parameterized as the dimensionless h_0, the amplitude of the (circularly polarized) signal that would be received if the star lay directly above or below the plane of the detector, with its spin axis pointing directly toward (or away from) the detector, so that $h_0 = 2C_{22}$. Such triaxial stars are often colloquially described as having "mountains," or having a dimensionless equatorial ellipticity ϵ defined in terms of its principal moments of inertia (I_{xx}, I_{yy}, I_{zz}):

$$\epsilon \equiv \frac{|I_{xx} - I_{yy}|}{I_{zz}}, \quad (3)$$

with the understanding that the star spins about the z-axis. The gravitational-wave amplitudes and equatorial ellipticities are then related by

$$h_0 = \frac{16\pi^2 G}{c^4}\frac{I_{zz}\epsilon f_{\rm rot}^2}{d}, \quad (4)$$

where $f_{\rm rot}$ is the rotational frequency and d is the star's distance. Yet another quantity that is often quoted is the mass quadrupole Q_{22}, a quantity with the same dimension as the moment of inertia, and one that appears directly in the mass quadrupole formalism for calculating gravitational-wave amplitudes:

$$Q_{22} = I_{zz}\epsilon\sqrt{\frac{15}{8\pi}}. \quad (5)$$

When applying these formulae, we will use a fiducial value $I_{zz}^{\rm fid} = 10^{38}\ {\rm kg\,m^2}$ for the moment of inertia.

We quote our results in terms of the ratio between minimum gravitational-wave detectable amplitude and the spin-down limit, which is given by:

$$h_{0,\rm sd} = \frac{1}{d}\left(\frac{5GI_{zz}}{2c^3}\frac{|\dot{f}_{\rm rot}|}{f_{\rm rot}}\right)^{1/2}, \quad (6)$$

which comes from the assumption that all rotational energy lost by the pulsar powers the gravitational-wave emission. This limit is surpassed when the minimum detectable gravitational-wave amplitude h_0 is smaller than $h_{0,\rm sd}$.

We also make a distinction between intrinsic and observed spin-downs of the pulsars we analyze. The observed spin-downs are affected by the transverse velocity of the source (Shklovskii 1970), and can differ substantially from the intrinsic ones (see Table 2). So when possible, we use the intrinsic spin-down to calculate the spin-down limit.

In the case of the narrowband search, a range of frequencies and spin-down rates is searched over, centered on the rotationally derived values, allowing for fractional deviations of up to a maximum value. For emission close to $2f_{\rm rot}$, this corresponds to ranges in search frequency $f_{\rm GW}$ and its first time derivative $\dot{f}_{\rm rot}$ of:

$$1 - \delta < \frac{f_{\rm GW}}{2f_{\rm rot}} < 1 + \delta, \quad (7)$$

$$1 - \delta < \frac{\dot{f}_{\rm GW}}{2\dot{f}_{\rm rot}} < 1 + \delta. \quad (8)$$

Previous narrowband searches used values of δ of the order of $\sim\mathcal{O}(10^{-4})$ motivated partly by astrophysical considerations for the gravitational-wave emission mechanism. In fact, Equations (7) and (8) can take into account the possibility that the gravitational wave is emitted by a free precessing biaxial neutron star (Jones & Andersson 2002) or the possibility that the star crust and core are linked by a torque that would enforce corotation. In the previous cases, the gravitational wave emitted would be a nearly monochromatic signal emitted at a slightly different frequency and spin-down with respect to the one observed from electromagnetic observations. Section 2 below gives further details of how these signal models are used by the various data analysis methods. We note that the values of δ chosen for the present search are sufficient to cover a parameter range roughly an order of magnitude greater than what is expected astrophysically by the above mechanisms.

2. Analysis Methods

Here, we briefly describe the analysis methods used in producing our results. We highlight any differences in the methods compared to those used in previous analyses (e.g., Abbott et al. 2019a, 2019b). For the analyses presented here, the methods are variously applied for two different signal models: (i) a signal emitted purely by the $l = m = 2$ mass quadrupole mode (i.e., a rigid triaxial rotator) at precisely, or

close to, twice the star's rotation frequency, and (ii) a signal emitted by one or both of the $l = m = 2$ and $l = 2$, $m = 1$ modes with components at precisely, or close to, once and twice the rotation frequency. For the searches that do not allow a narrow band of frequencies and frequency derivatives, we assume that the best-fit radio timing model gives a phase coherent solution over the full range of the gravitational-wave data, and we do not account for any uncertainties on the radio-derived values.

The methods for targeted searches assume that the gravitational-wave signal precisely tracks the radio-derived phase evolution, and therefore only a single phase evolution template is required. In the following sections we describe the three methodologies employed in this paper: *the time-domain Bayesian method*, *the $\mathcal{F}/\mathcal{G}$-statistic method*, and *the 5n-vector method*. The first two methods coherently analyze O1, O2, and O3 data,[214] while the latter, along with the *5n-vector narrowband* search, uses only O3 data (see Section 3.1 for more details on GW data).

The analyses also consider the occurrence of pulsar glitches using different methodologies. For the Crab pulsar (J0534+2200), there were five glitches over the analysis period (see Section 3.2.2 and Section 2.1.1 of Abbott et al. 2019a); for the Vela pulsar, there was a glitch between O2 and O3a (Gancio et al. 2020 and references therein).

2.1. Time-domain Bayesian Method

As described in Dupuis & Woan (2005), for each pulsar, this method preprocesses the raw gravitational-wave strain, which is then used as the input to a Bayesian parameter estimation code (Pitkin et al. 2017). The parameter estimation uses a nested sampling algorithm, as implemented in the LALINFERENCE package (Veitch & Vecchio 2010; Veitch et al. 2015), to infer the unknown gravitational-wave parameters of the expected signal, which depend on the signal model described Section 1.2. In contrast to the previous searches for the $l = m = 2$ mode using this method (e.g., Aasi et al. 2014; Abbott et al. 2017d, 2019a), which have directly inferred the gravitational-wave amplitude h_0 for each signal, we now parameterize the amplitude in terms of the mass quadrupole Q_{22} and pulsar distance d as in Equations (4) and (5). The distances are given Gaussian prior probability distributions, with mean and standard deviation values taken from the distance estimates for the pulsars (see Table 2). The Q_{22} prior distribution is chosen to be flat over the range $[0, 5 \times 10^{37}]$ kg m^2, and zero outside this range. This is not a physically motivated range, but is chosen to be more than an order of magnitude larger than the largest upper limit found in Abbott et al. (2019a).

In the gravitational-wave analysis, we assume that the signal evolution is affected by a glitch in the same way as that observed with the electromagnetic pulses, except that each glitch may introduce a phase offset between the electromagnetic and gravitational-wave signals. These unknown phase offset parameters are included in the parameter inference. Three of the Crab pulsar glitches described in Section 3.2.2 occurred between O2 and O3, so it would be impossible to use our gravitational-wave data to distinguish different phase offsets for each of these glitches. Therefore, only one phase offset parameter is required to account for the three glitches. During this work an error was found and fixed in the analysis when accounting for the glitch behavior during the parameter inference stage. This led to the time-domain Bayesian results for the Crab and Vela pulsar from Abbott et al. (2019a) being updated to those now given in Abbott et al. (2020a).

As described in Section 3.2.2, for the Vela pulsar, we have a coherent timing model over only the period of O3a. Therefore, we have to combine the results from an analysis on O1 and O2 data with that from O3a in a semi-coherent manner. This also means that we do not need to account for the Vela pulsar glitch between O2 and O3a with the inclusion of an additional phase offset. Because of the bug described above, an analysis of combined O1 and O2 data used in Abbott et al. (2019a) was repeated for this work, but with the corrected code and (for the single harmonic search) with parameter inference on Q_{22} and distance instead of h_0. For the single harmonic search, the joint posterior on Q_{22} and ι was fitted with a multivariate Gaussian mixture model (using the `BayesianGaussianMixture` function within scikit-learn; Pedregosa et al. 2011), allowing a maximum of 20 components. This mixture model was then used as the prior on these parameters when analyzing O3a data. For the dual-harmonic search, the mixture model was fitted to the joint C_{21}, C_{22}, and ι posterior.

2.2. Time-domain $\mathcal{F}/\mathcal{G}$-statistic Method

The time-domain $\mathcal{F}/\mathcal{G}$-statistic method uses the $\mathcal{F}$ and $\mathcal{G}$ statistics developed in Jaranowski et al. (1998) and Jaranowski & Królak (2010). The $\mathcal{F}$-statistic is used when the amplitude, phase, and polarization of the signal are unknown, whereas the $\mathcal{G}$-statistic is applied when only amplitude and phase are unknown, and the polarization of the signal is known (as described in Section 2.4). The methods have been used in several analyses of LIGO and Virgo data (Abadie et al. 2011; Aasi et al. 2014; Abbott et al. 2017d).

In this method a signal is detected in the data if the value of the $\mathcal{F}$- or $\mathcal{G}$-statistic exceeds a certain threshold corresponding to an acceptable false-alarm probability. We consider the false-alarm probability of 1% for the signal to be significant. The $\mathcal{F}$- and $\mathcal{G}$-statistics are computed for each detector and each inter-glitch period separately. The results from different detectors or different inter-glitch periods are then combined incoherently by adding the respective statistics. When the values of the statistics are not statistically significant, we set upper limits on the amplitude of the gravitational-wave signal.

2.3. 5n-vector Method

The frequency-domain 5n-vector method has been introduced in Astone et al. (2010, 2012) and used in several analyses of LIGO and Virgo data (Abadie et al. 2011; Aasi et al. 2014; Abbott et al. 2017d, 2019a). It is also the basis of the narrowband pipeline described in Section 2.5. In this paper it has been applied to a subset of three pulsars: J0711−6830, the Crab pulsar, and the Vela pulsar.

In contrast to past analyses—which used resampling—the barycentric, spin-down, and Einstein delay corrections are done by heterodyning the data, using the band sampled data framework (Piccinni et al. 2019). This significantly reduces the computational cost of the analysis, which drops from about half of a CPU-day to a few CPU-minutes per source per detector. A detection statistic, based on the matched filter among the 5n-vectors of the data and the signal, is obtained and used to estimate the significance of an analysis result. Upper limits are computed using the approach first introduced in Aasi et al. (2014).

[214] With the exception of the Vela pulsar.

As in Abbott et al. (2019a), two independent analyses have been done assuming that the emission takes place at two times the star rotation frequency and at the rotation frequency (according to the model described in Jones 2010). While performing this analysis, we identified an incorrect choice for the range of amplitudes used to inject simulated signals in the O2 analysis of the pulsar J0711−6830; see Abbott et al. (2020a) for more details. This affects only the upper limit computation at the rotation frequency for J0711−6830, and the corrected value is given in Abbott et al. (2020a).

2.4. Restricted Orientations

As with previous analyses, all of the pipelines produce results for the Crab and Vela pulsars based on two different assumptions. The first is that the orientation of the pulsar is unknown, so a uniform prior over the inclination and polarization angle space is used. The second uses estimates of the source orientation based on X-ray observations of the pulsar wind nebulae tori (Ng & Romani 2004, 2008), which are included in the pipelines as narrow priors on inclination and polarization angle (effectively defining the polarization state of the signal), as given in Table 3 of Abbott et al. (2017d).

2.5. 5n-vector Narrow Band

The *5n-vector narrowband pipeline* described in Mastrogiovanni et al. (2017) uses the 5*n*-vector method of Astone et al. (2010, 2012) and expands it to a narrow frequency and spin-down range around the source ephemerides values. This pipeline has previously been applied to the O1 and O2 data sets in Abbott et al. (2017e, 2019b) permitting the analysis of pulsars for which ephemerides were not accurately known.

In contrast to Abbott et al. (2019b), we now combine the matched filter's results between the detectors using weight factors computed from the power spectral density: each data set is weighted inversely by the median noise power in the analyzed frequency band. This allows the analysis to depend most strongly on the most sensitive data set. The final step is to select the local maximum of a detection statistic every 10^{-4} Hz over the spin-down values considered. Within this set of points in the parameter space, we select as outliers those with a *p*-value below a 0.1% threshold (taking into account the number of trials).

This method targets pulsars J0711−6830, Crab, and Vela. For J0711−6830 and Vela, we analyzed 6 months of data, so the frequency and spin-down resolutions were 6.5×10^{-8} Hz and 4.3×10^{-15} Hz s^{-1}, respectively. For Crab, the resolutions were 1.0×10^{-7} Hz and 1.1×10^{-14} Hz s^{-1} since we considered only data preceding the glitch (∼115 days). The narrowband resolutions relate to the natural discretization step of the discrete Fourier transform. The resolution ensures that a nearly monochromatic gravitational-wave signal, emitted in the explored parameter space, is subject to a maximum loss of signal-to-noise ratio of ∼36% (Ransom et al. 2002). Note that, in order to reduce this loss, a half-bin interpolation of the Fourier transform is implemented in the code.

For each pulsar, we analyze a gravitational-wave frequency and spin-down range set to within 0.4% of the ephemerides frequency and spin-down. This corresponds[215] to $\delta \sim 2 \times 10^{-3}$ in Equations (7) and (8). With respect to the O2 narrowband search, this corresponds to a volume explored in the frequency/spin-down range that is four times larger. We report the frequency and spin-down bands explored in Table 1.

Table 1
Frequency/Spin-down Ranges Explored in the 5*n*-vector Narrowband Search

Pulsar	$\Delta f_{\rm GW}$ (Hz)	$\Delta \dot{f}_{\rm GW}$ (Hz s^{-1})	n_f	$n_{\dot f}$
J0534+2200[a] (Crab)	0.24	3.0×10^{-12}	3.8×10^{6}	270
J0711−6830	0.72	8.4×10^{-15}	1.2×10^{7}	3
J0835−4510 (Vela)	0.10	1.4×10^{-13}	1.4×10^{6}	33

Notes. Second and third columns: frequency and spin-down ranges explored, respectively. Fourth and fifth columns: number of values in frequency and number of spin-down values considered, respectively. The total number of templates per pulsar is $n_f \times n_{\dot f}$.
[a] Only data before the glitch reported in Shaw et al. (2019) are considered.

Finally, for computing the 95% confidence level upper limits on the gravitational-wave amplitude h_0, we use the procedure described in Abbott et al. (2019b) to inject several simulated gravitational-wave signals in each 10^{-4} Hz sub-band. For each sub-band, we set the upper limit at the strain amplitude for which 95% of the injected signals are recovered.

3. Data Sets Used

3.1. Gravitational-wave Data

We use a combination of data from the first, second, and third observing runs of the Advanced LIGO (Aasi et al. 2015) and Virgo (Acernese et al. 2015) gravitational-wave detectors. For O1 and O2, only data from the LIGO Hanford (H1) and LIGO Linvingston (L1) detectors have been used, while for O3, data from both LIGO detectors and the Virgo (V1) detector have been used. The O1 data cover the period from 2015 September 11 to 2016 January 19, with duty factors of ∼51% and ∼60% for L1 and H1, respectively. The O2 data cover the period from 2016 November 30 to 2017 August 25, with duty factors of ∼57% and ∼59% for L1 and H1, respectively (including commissioning breaks). For O3, a period from 2019 April 1 to 2019 October 1 was designated O3a, prior to a one month commissioning break. O3a had duty factors of ∼76%, ∼71%, and ∼76% for L1, H1, and V1, respectively.

The data and subsequent upper limits are subject to uncertainty in the calibration of the instruments. The calibration uncertainty varies in amplitude and phase over the course of a run. We do not account for these variations in our results (see below), but we expect them to have a negligible impact on the results. For more details of the O1 and O2 data and calibration used in these searches, see the discussions in Abbott et al. (2017d, 2019a). The full raw strain data from the O1 and O2 runs are publicly available from the Gravitational Wave Open Science Center[216] (Vallisneri et al. 2015; Abbott et al. 2019h). For the LIGO O3a data set, the time-domain Bayesian and $\mathcal{F}/\mathcal{G}$-statistic methods use the "C01" calibration for LIGO, while the 5*n*-vector methods use the "C00" calibration. The C01 calibration has estimated maximum amplitude and phase uncertainties of 7% and 4 deg, respectively (Sun et al. 2020), while the C00 estimates are 8% and 5 deg. For the Virgo O3a data set, all of the pipelines use the "V0" calibration with estimated maximum amplitude and phase uncertainties of 5% and 3 deg, respectively.

[215] Note that for the frequency range of J0711−6830, we used a value of 0.2% with a corresponding $\delta \sim 1 \times 10^{-3}$. This was due to the constraints given by the 1 Hz subsampling procedure.

[216] https://www.gw-openscience.org/data

Table 2
Properties of the Pulsars in This Search

Pulsar	$f_{\rm rot}$ (Hz)	$\dot{f}_{\rm rot}$ (Hz s^{-1})	$\dot{f}_{\rm rot}^{\rm int}$ (Hz s^{-1})	Distance (kpc)	Spin-down luminosity (W)
			Young pulsars		
J0534+2200 (Crab)	29.6	-3.7×10^{-10}	…	2.0 ± 0.5[a]	4.5×10^{31}
J0835−4510 (Vela)	11.2	-2.8×10^{-11}[b]	…	$0.287^{+0.019}_{-0.017}$[c]	6.9×10^{29}
			Recycled pulsars		
J0437−4715	173.7	-1.7×10^{-15}	-4.1×10^{-16}	0.15679 ± 0.00025[d]	2.8×10^{26}
J0711−6830	182.1	-4.9×10^{-16}	-4.7×10^{-16}	0.110 ± 0.044[e]	3.4×10^{26}
J0737−3039A	44.1	-3.4×10^{-15}	…	$1.15^{+0.22}_{-0.16}$[f]	5.9×10^{26}

Notes. If an intrinsic rotation period derivative $\dot{P}_{\rm rot}^{\rm int}$ is available from the Australia Telescope National Facility (ATNF) Pulsar Catalog (Manchester et al. 2005), and is significantly different from the observed value, then this is converted into an intrinsic frequency derivative via $\dot{f}_{\rm rot}^{\rm int} = -f_{\rm rot}^2 \dot{P}_{\rm rot}^{\rm int}$ and is quoted here. For J0437−4715 and J0711−6830, this intrinsic frequency derivative will be used to calculate the spin-down luminosity and the spin-down limits in Table 3.

[a] Kaplan et al. (2008).

[b] The $\dot{f}_{\rm rot}$ value given here is for the observation span used in this work; however, the spin-down limit shown in Table 3 uses the long-term value of $f_{\rm rot} = -1.57 \times 10^{-11}$ Hz s^{-1} as given in the ATNF Pulsar Catalog (Manchester et al. 2005).

[c] This distance is from Dodson et al. (2003), although the Bayesian analysis described in Section 2.1 uses a symmetric distance uncertainty of 0.288 ± 0.018 kpc.

[d] Reardon et al. (2016).

[e] This distance is based on dispersion measure from the Yao et al. (2017) model, with a 40% uncertainty assumed.

[f] This distance is from Deller et al. (2009), although the Bayesian analysis described in Section 2.1 uses a symmetric distance uncertainty of 1.18 ± 0.19 kpc.

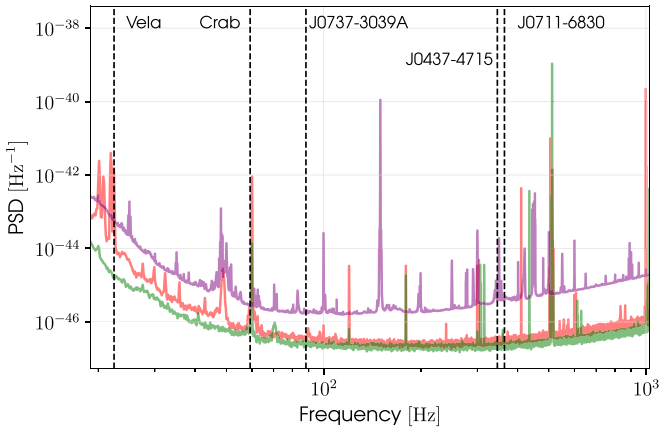

Figure 1. O3a noise PSD for H1, L1, and V1 shown in red, green, and purple. The H1 and L1 PSDs are calculated during a time period of optimal performance for the detector, while the Virgo PSD is averaged over the run. The vertical dashed lines indicate the searched frequency region for each of the five pulsars.

For the Bayesian analysis, we estimate that the statistical uncertainty on the upper limits due to the use of a finite number of posterior samples is on the order of 1%. For the 5n-vector analysis, the statistical uncertainty on the upper limits has been estimated to be 1%–3% depending on the target.

Besides calibration uncertainties, the detectors' data sets are polluted by several noise disturbances. Some of these disturbances are qualitatively visible as spikes or other deviations from smoothness in the noise power spectral densities (PSDs) for L1, H1, and V1 in Figure 1 with respect to the five pulsars frequency searched.

3.2. Electromagnetic Data

The timing solutions used in our gravitational-wave searches have been derived from electromagnetic observations of pulsars. These pulsars' basic properties are given in Table 2, and are further explained in the next subsections.

3.2.1. Recycled Pulsars

The pulsars J0437−4715 and J0711−6830 are monitored by the Parkes Pulsar Timing Array project (PPTA; Manchester et al. 2013). The timing models for these pulsars were determined using data from the second data release of the PPTA (DR2; Kerr et al. 2020). The model parameters were fit using TEMPO2 (Hobbs et al. 2006), with the stochastic red noise and dispersion measure (DM) variations characterized as power-law processes and included in the fit (as the phases of a series of Fourier components for each power law). The power-law parameters (amplitude and spectral index) and white noise properties were determined using the ENTERPRISE (Ellis et al. 2019) Bayesian pulsar timing analysis software. The noise models were consistent with those published with DR2. The timing stability for the pulsars J0437−4715 and J0711−6830 is such that the weighted rms timing residuals (excluding DM variations, but including spin noise) are 0.006% and 0.035% of a pulse period, respectively, over a span of ∼14 yr.

The timing model for the pulsar J0737−3039A was developed using a combination of archival observations taken at various frequencies ranging between 604 and 1410 MHz by the CSIRO 64 m Parkes radio telescope from 2004 to 2014, and 835 MHz observations performed by the upgraded Molonglo Observatory Synthesis Telescope (Bailes et al. 2017) between 2015 and 2018. Times of arrival (TOAs) at each observing band were computed via the standard cross-correlation technique, with each frequency band using its own template. They were then analyzed using the TEMPONEST (Lentati et al. 2014) Bayesian pulsar timing plugin to TEMPO2, which allowed us to measure the pulsar's deterministic and stochastic (red and white noise) properties simultaneously. The post-fit timing residuals have a weighted rms of ∼24 μs, corresponding to about 0.01% of a pulse period over ∼15 yr.

3.2.2. Young Pulsars

As mentioned in Section 2, the time-domain Bayesian and $\mathcal{F}/\mathcal{G}$-statistic methods coherently analyze all O1, O2, and O3a

Table 3
Limits on Gravitational-wave Amplitude, and Other Derived Quantities, for the Three Targeted Searches

Pulsar name (J2000)	h_0^{sd} (10^{-26})	Analysis method	$C_{21}^{95\%}$ (10^{-26})	$C_{22}^{95\%}$ (10^{-27})	$h_0^{95\%}$ (10^{-26})	$Q_{22}^{95\%}$ (10^{32} kg m^2)	$\epsilon^{95\%}$	$h_0^{95\%}/h_0^{sd}$
Young pulsars[a]								
J0534+2200[b] (Crab)	140	Bayesian	12.7(7.9)	6.3(5.6)	1.5(1.2)	6.6(5.7)	$8.6(7.4) \times 10^{-6}$	0.010(0.009)
		$\mathcal{F}/\mathcal{G}$-statistic	8.9(6.2)	7.9(7.1)	1.9(1.5)	7.9(6.3)	$10(8.1) \times 10^{-6}$	0.014(0.011)
		5n-vector	15.9(12.4)	…	3.0(2.9)	12.6(12.1)	$16.3(15.7) \times 10^{-6}$	0.021(0.021)
J0835−4510 (Vela)	330	Bayesian	1100(980)	120(84)	22(17)	91(73)	$12.0(9.5) \times 10^{-5}$	0.067(0.052)
		$\mathcal{F}/\mathcal{G}$-statistic	1470(1370)	116(48)	23(12)	96(50)	$12.4(6.4) \times 10^{-5}$	0.070(0.036)
		5n-vector	1700(1400)	…	24(24)	100(102)	$13.0(13.2) \times 10^{-5}$	0.073(0.073)
Recycled pulsars								
J0437−4715	0.79	Bayesian	2.2	4.1	0.78	0.0074	9.5×10^{-9}	0.99
		$\mathcal{F}/\mathcal{G}$-statistic	2.1	7.2	0.86	0.0082	11.0×10^{-9}	1.1
		5n-vector	…	…	…	…	…	…
J0711−6830	1.2	Bayesian	2.6	3.5	0.82	0.0064	8.3×10^{-9}	0.68
		$\mathcal{F}/\mathcal{G}$-statistic	2.4	9.4	0.98	0.0059	7.7×10^{-9}	0.82
		5n-vector	2.9	…	0.91	0.0053	7.2×10^{-9}	0.76
J0737−3039A	0.62	Bayesian	5.9	3.3	0.69	0.80	1.0×10^{-6}	1.1
		$\mathcal{F}/\mathcal{G}$-statistic	3.0	1.2	0.99	1.10	1.4×10^{-6}	1.6
		5n-vector	…	…	…	…	…	…

Notes. Parameters for the pulsars can be found in Table 2.
[a] For J0534+2200 and J0835−4510, the results in parentheses are those when using restricted priors on the pulsar orientation.
[b] For the 5n-vector results, only data from the O3a run were used for all three pulsars.
(This table is available in its entirety in machine-readable form.)

data, while the 5n-vector method only uses O3a data. Therefore, for the Crab pulsar, two timing solutions were obtained as described below: one using radio observations overlapping with O3a and another using data overlapping the period between the start of O1 and the end of O3a.

For the 5n-vector search, the timing model for the Crab pulsar was created using pulse TOAs measured at the Jodrell Bank Observatory (JBO) between 2019 April and October. The data set contains 352 TOAs obtained with the 42 ft telescope, using a 10 MHz wide band, centered on 610 MHz. In order to carefully track DM variations in the direction of the Crab pulsar, we include an additional 134 TOAs obtained with the 76 m Lovell telescope, using a 384 MHz wide band, centered on 1520 MHz. Further details of JBO observations can be found in Lyne et al. (2015).

To account for the effects of timing noise on the Crab pulsar's rotation, we fit the TOAs, using TEMPO2, with a Taylor series of the spin frequency comprising terms up to 12th order. The Crab pulsar exhibits strong variations in DM, primarily due to the dynamics of the supernova remnant in which the pulsar resides (e.g., McKee et al. 2018). In order to mitigate the effects of DM variations on the measured TOAs from the Crab pulsar, we piecewise fit the DM at 22 epochs within the O3a period, meaning the value of DM in the timing model is updated every ∼8 days. Finally, we include in the timing model the effects of a moderately sized spin-up glitch that occurred during an observation of the Crab pulsar on 2019 July 23 (Shaw et al. 2019). Applying this timing model to the measured TOAs, the resulting timing residuals have an rms value of ∼67 μs, corresponding to 0.2% of one pulse period.

The second timing model for the Crab pulsar, used for the time-domain Bayesian and $\mathcal{F}/\mathcal{G}$-statistic searches, was created covering the entire period from 2015 August to 2019 October. In this case, the data set comprises 2478 TOAs measured with the 42 ft telescope and 858 TOAs measured with the Lovell telescopes at the same bandwidths and center frequencies as stated above, forming a total of 3336 observations. For these data, the timing noise was modeled using a Taylor series of the spin frequency with terms up to 12th order, in combination with 100 harmonically related sinusoids, implemented using the FITWAVES functionality in TEMPO2. A piecewise model of the DM was also included, comprising DM values at 110 epochs (approximately every 14 days). Over this time period, the Crab pulsar underwent five spin-up glitches including the 2019 July glitch and the largest glitch observed to date in the Crab pulsar, which occurred in 2017 November (Shaw et al. 2018). These two glitches and their recoveries are included in the timing model. The remaining three glitches were sufficiently small as to be fully described by the other parameters together with the timing noise and so are not specifically modeled here. The residuals resulting from this timing model have an rms value of ∼21 μs, corresponding to 0.06% of one pulse period.

A timing model for the Vela pulsar was created using pulse TOAs from the Mt Pleasant 26 m radio observatory near Hobart, Tasmania. The entire O3a observing period was covered, and the center frequency was 1376 MHz with a bandwidth of 64 MHz. The single-pulse observations were integrated to 1 hr, and TEMPO2 was used to create an ephemeris from those 464 TOAs. A Taylor series to the fourth derivative was used to get an rms of ∼50 μs, which is 0.06% of the pulse period.

4. Analysis Results

4.1. Targeted Searches

The results from the targeted searches for all five pulsars are summarized in Table 3 with the three different pipelines presented together for ease of comparison.

No evidence for a signal was observed from any of the five pulsars in either of the harmonics studied, so as with previous

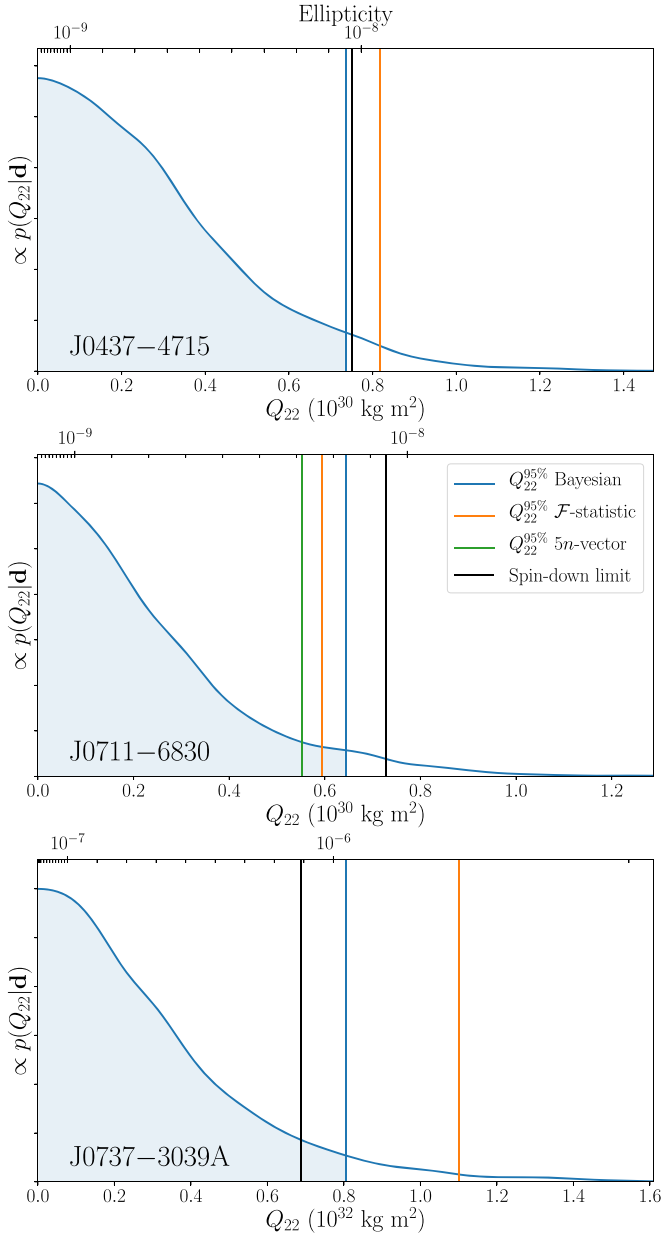

Figure 2. Posterior distributions on Q_{22} for the Bayesian analysis of the three recycled pulsars. Also shown as vertical lines are the 95% credible upper limits from the three different pipelines and the spin-down limits. The upper axes show the equivalent limits on the fiducial ellipticity.

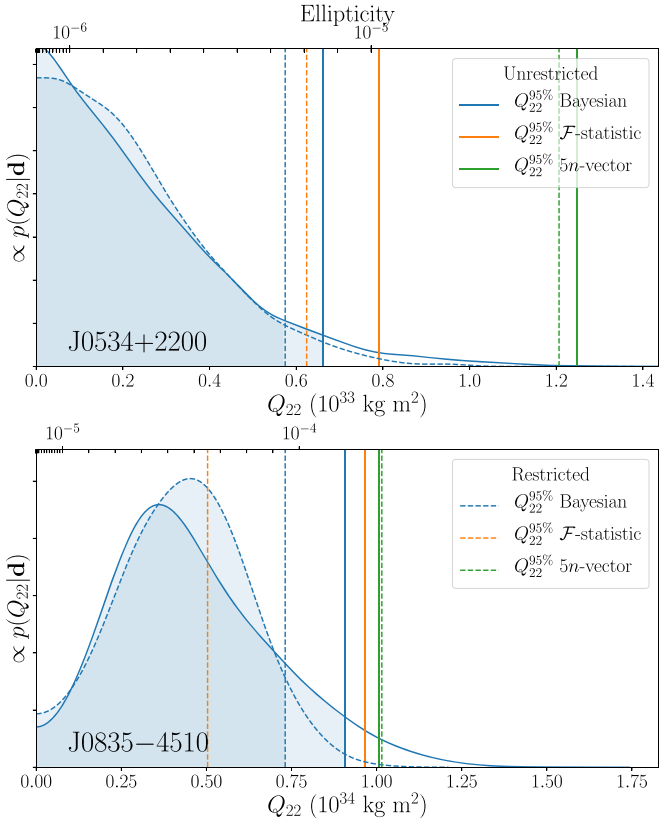

Figure 3. Posterior distributions on Q_{22} for the Bayesian analysis of the two young pulsars Crab and Vela. The solid lines show the results when not using prior restrictions on the pulsar orientations (see Section 2.4), while those with restrictions are shown as the dashed lines. Also shown as vertical lines are the 95% credible upper limits from the three different pipelines. The upper axes show the equivalent limits on the fiducial ellipticity.

analyses, we present the results as 95% credible upper limits on the gravitational-wave amplitudes: C_{21} and C_{22} for the dual-harmonic search, and h_0 for the single harmonic search. For the single harmonic search, using Equations (4) and (5), we place equivalent limits on the mass quadrupole Q_{22} and fiducial ellipticity ϵ. The posterior distributions on Q_{22} for the Bayesian analysis, along with the point estimate upper limits from the $\mathcal{F}/\mathcal{G}$-statistic and 5n-vector pipelines, are shown in Figure 2 for the three recycled pulsars and Figure 3 for Crab and Vela. In Figure 3 the upper limits are shown using both restricted-orientation and unrestricted priors as described in Section 2.4.

Despite the analysis pipelines being largely independent, and the statistical procedures used to derive upper limits being different, there is a broad agreement among the different pipelines. One source of differences, however, comes from the pipelines not all using the same data sets. The 5n-vector search analyzed only O3a data while the Bayesian and $\mathcal{F}/\mathcal{G}$-statistic search coherently (or semi-coherently in the case of the Vela pulsar) combined data from O1, O2, and O3a. The methods of combining data for the Vela pulsar analysis are discussed in Section 2.

Another source of differences is that the Bayesian analysis does not assume a fixed distance, but instead includes it as a parameter to be estimated from the data. Therefore, limits on Q_{22} and h_0 are computed marginalizing over the distance, rather than assuming a fixed value. In general, the distance posterior distributions match their priors well but with a small bias toward larger values when the distance priors are wide. However, for J0711−6830 the bias is more obvious with the peak in the distance posterior being at a value approximately 20% larger than that of the prior. This biasing of the distance is due to our choice of a flat prior on Q_{22}, which is not an uninformative distribution; i.e., there is much more prior weight for large Q_{22} values, disfavoring smaller distances.

In the discussions below, we will generally refer to the most stringent, i.e., lowest, limit from the different searches and will discuss only the single harmonic ($l = m = 2$ mass quadrupole) and unrestricted-orientation priors results in detail.

4.1.1. Recycled Pulsars

We surpassed for the first time the spin-down limit for J0437−4715 and J0711−6830. For J0437−4715 our 95% upper

limits are just below the spin-down limit, and for J0711−6830 it is at ∼70% of the spin-down limit. For J0711−6830 this equates to less than half of the intrinsic spin-down energy loss attributable to gravitational-wave emission. For these two pulsars, these limits provide constraints that are below the fiducial ellipticity of 10^{-8}, which was previously surpassed for only J0636+5129 (Abbott et al. 2019a).

4.1.2. J0737−3039A

For J0737−3039A our limits are only just above the spin-down limit, and would easily surpass it assuming a slightly larger moment of inertia. For this pulsar, despite having a similar spin-down limit to two of the recycled pulsars, its significantly lower frequency and larger distance leads to a limit on fiducial ellipticity that is around 10^{-6}.

4.1.3. Young Pulsars

The inclusion of O3a data for the Crab and Vela pulsars does not significantly improve the results compared to previous analyses (Abbott et al. 2019a, 2020a), because the detector sensitivity improvements achieved for the O3 run via quantum squeezing were greatest at high frequencies (Acernese et al. 2019; Tse et al. 2019).

We obtain limits on the GW emission from the Crab pulsar at 1%–2% of the spin-down limit regardless of prior choice, corresponding to a limit on fiducial ellipticity of $\epsilon \sim 10^{-5}$. For the Vela pulsar, we obtain limits on the GW emission that are less than ∼7% of the spin-down limit, corresponding to a fiducial ellipticity of $\epsilon \lesssim 10^{-4}$. As seen in Figure 3, the posterior distribution on Q_{22} peaks away from but is not disjoint from zero. Such a distribution is not uncommon for pure Gaussian noise, but could also be due in part to spectral contamination observed near twice the Vela pulsar's rotation frequency in all detectors (see Figures 1 and 5).

4.2. 5n-vector Narrow Band

The narrowband search found no evidence for GW emission from J0711−6830, the Crab pulsar, or the Vela pulsar, although several analysis outliers were found for two of these pulsars.

For J0711−6830 there were 19 outliers. Sixteen outliers clustered at the boundaries of the analyzed frequency band and were due to artifacts created by the band extraction close to the integer frequency of 364 Hz. These artifacts are created due to subsample processes at 1 Hz. The remaining three outliers, labeled as C17, C18, and C19 (see Figure 4, top panel), were found by the narrowband pipeline with a p-value of $\sim 1.2 \times 10^{-7}$, which when rescaled for the number of trials corresponds to a p-value of $\sim 5.0 \times 10^{-4}$. In order to assess the significance of the outliers, we performed a narrowband search for J0711−6830 using the same setup for the rotational parameters but using an "off-source" sky position. This procedure would effectively blind the analysis to the presence of a possible astrophysical signal, thus allowing us to build an empirical noise-only distribution of the detection statistic, which can be used to reassess the outliers' significances. From this analysis we found that the p-values of two of the three outliers were above the narrowband ceiling of 0.1% (C17 and C19), while the value for C18 was 0.06%. This test indicated that by re-assigning the significance with the off-source method, two of the outliers would not have passed the narrowband threshold for candidate selection and hence could be due to low-level noise instrumental artifacts.

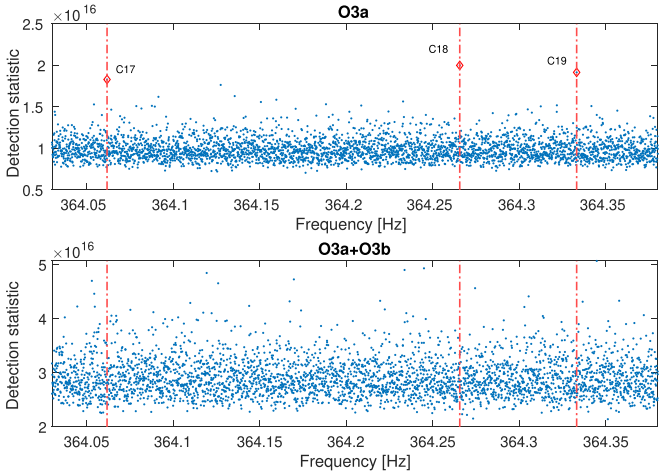

Figure 4. Top panel: detection statistic obtained from the narrowband analysis of J0711−6830 using O3a data. The outliers are indicated with red diamonds and red vertical lines. Bottom panel: detection statistic obtained from the narrowband analysis for J0711−6830 using the full O3 data set. The frequencies of the original O3a outliers are indicated by red vertical lines.

The three outliers were followed-up by two of the targeted pipelines. For the three outliers, the time-domain Bayesian pipeline found a strong preference for the hypothesis that the data (with a bandwidth of 1/60 Hz centered on the outlier) was consistent with Gaussian noise compared to a hypothesis that it also contained signals coherent between detectors. Specifically, the Bayes factors recovered for the signal versus noise hypothesis were $<10^{-4}$; thus they are likely the noise origin for all of these outliers. Additionally, for C17 and C19, the pipeline recovered a maximum posterior on h_0 of 1.6×10^{-26} and 8.5×10^{-27}. As argued in the case of the Vela pulsar in Section 4.1.3, this can be related to the presence of instrumental noise contributions.

The 5n-vector targeted pipeline also performed a follow-up of the most significant of the three outliers (C18), with frequency ∼364.25 Hz, using software injections with an amplitude set to that of one of the recovered outliers. The pipeline found that the distribution of the software injection's detection statistic was compatible with the value displayed by the outlier. More precisely, for a set of 50 injected signals, it found an average critical ratio $\overline{\mathrm{CR}} = 7.0$ with a standard deviation of 3.2, to be compared with a value 8.5 found for the actual analysis candidate. In the absence of any signal, the noise average critical ratio was found to be $\overline{\mathrm{CR}} = 0.3 \pm 1.3$.

Given that the previous tests did not conclusively establish the noise origin of the outliers, we performed a narrowband analysis using the full O3 LIGO data set (C00 calibration). If the outliers were due to a real continuous wave signal, we would have expected to see them as more significant in this analysis. Figure 4 compares the detection statistics obtained from the narrowband analysis using only O3a data and the full O3 data set. We see that the outliers found in the O3a run are no longer present when using the full run, which is inconsistent with an astrophysical signal.

Finally, for the Vela pulsar, we found four outliers, but these are due to noise disturbances in the data; see Figure 5. One of the candidates was due to the left sidebands of a known H1 disturbance at 22.347 Hz together with a noise disturbance

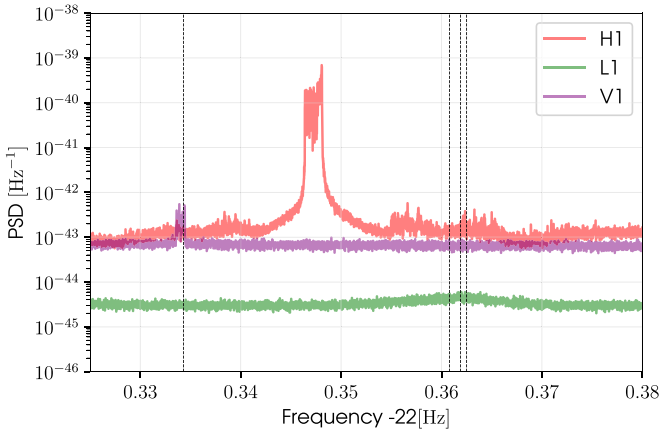

Figure 5. Power spectral density of H1 (red), L1 (green), and V1 (purple) after the correction for the CW modulations. The dashed vertical lines mark the frequencies of the four Vela outliers affected by instrumental disturbances.

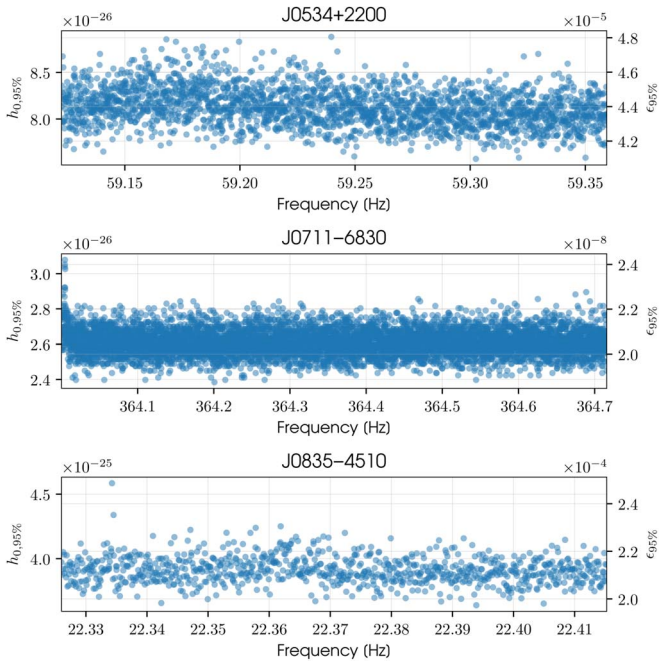

Figure 6. The graphs show the 95% confidence level upper limits on the gravitational-wave amplitude h_0 and ellipticity ϵ for the three pulsars analyzed in the narrowband analysis. From top to bottom, the upper limits are shown for Crab, J0711−6830, and Vela. The contribution of the H1 and V1 noise disturbances are clearly visible in Vela's upper limits.

known in V1 at 22.333 Hz. The other three outliers were due to the right sidebands of the H1 disturbance and an L1 broadband noise disturbance around 22.365 Hz.

Hence we computed the 95% confidence level upper limits on the gravitational-wave amplitudes h_0 and the corresponding limits on the fiducial ellipticities, as shown in Figure 6. For pulsar J0711−6830 we obtain median values of the upper limit on the amplitude h_0 and the ellipticity over the analyzed frequency band of 2.6×10^{-26} and 2.0×10^{-8}, respectively. Unfortunately, the narrowband pipeline does not surpass the spin-down limit for this pulsar.

For the Crab and Vela pulsars, we obtain median values for the upper limit on h_0 of 8.1×10^{-24} and 3.90×10^{-25}, while the corresponding median upper limits on the fiducial ellipticities are 4.4×10^{-5} and 2.0×10^{-4}, respectively. These upper limits are factors of 1.6 and 2.25 better than the upper limit obtained with O2 data in Abbott et al. (2019b). This improvement has been partially made possible by the inclusion of Virgo data and the slightly improved sensitivities in O3 for the two LIGO detectors. Another major contribution, however, comes from the new PSD-weighted analysis that can account for data having different PSDs.

5. Discussion

For the first time, we have been able to surpass the spin-down limit of a recycled pulsar. This achievement is significant for gravitational-wave searches from known pulsars for two reasons. First, the upper limits we have set on the ellipticities of these (rapidly rotating) stars are very small (around 10^{-8}), a consequence of the scaling of wave amplitude with ellipticity and spin frequency, $h_0 \sim \epsilon f^2$. Second and more crucial, recycled pulsars have quite a different evolutionary history from younger, more slowly spinning pulsars, as they are believed to have acquired their high spin frequencies in a prolonged period of accretion from a binary companion. This sustained accretion can lead, in principle, to non-axisymmetric deformation of the star.

Several such accretion-specific deformation mechanisms are known. One possibility was first noted by Bildsten (1998), who argued that temperature asymmetries in the crust of an accreting star would produce lateral variations in the locations of the transition layers between one nuclear species and the next, a suggestion that has since been examined in more detail (Osborne & Jones 2020; Singh et al. 2020; Ushomirsky et al. 2000). Another possibility is that the accretion process "buries" the star's magnetic field, so that a very strong *internal* field, much larger than the external field of $\sim 10^9$ G inferred from a typical recycled pulsar, distorts the star (Vigelius & Melatos 2009). Alternatively, it has been proposed that the changing shape of a centrifugally distorted star could cause the crust to crack, either during the initial spin-up phase (Fattoyev et al. 2018), or during the later (post-accretion) spin-down phase (Baym & Pines 1971). The ellipticity would be generated if this cracking were to occur in a sufficiently non-axisymmetric way. As a caveat, it should be noted that recycled pulsars are believed to be old, with ages $\sim 10^9$ yr, providing much time for annealing of non-axisymmetric distortions.

One can convert our upper limits on ellipticity into approximate upper limits on the strain in the crust, or, alternatively, on the strength of the internal magnetic field, with the understanding that the limits apply only to the part of the strain or magnetic field that sources a *quadrupolar* deformation of the star.

Assuming crustal strain u, using Equation (5) of Ushomirsky et al. (2000), we have

$$\epsilon \approx 10^{-7} \frac{u}{10^{-2}}. \tag{9}$$

To give two specific examples, this corresponds to a best upper limit on the strain in the crust of the Crab pulsar of $u \approx 0.86$ (using the nonrestricted priors), while for J0711−6830, we have a best upper limit of $u \approx 7.2 \times 10^{-4}$. This is to be compared with estimates of the breaking strain as high as 0.1 from the molecular dynamics simulations of Horowitz & Kadau (2009; see also the semi-analytical calculations of Baiko & Chugunov 2018). It should be noted however that application of such

results to a real neutron star requires extrapolation through many orders of magnitude in both size and temporal duration as compared to the molecular dynamics simulations, so caution should be exercised.

This strain upper limit also underlines the significance of our new results for the recycled pulsars. While the spin-down limit for the Crab pulsar was surpassed some years ago (Abbott et al. 2008), the necessary crustal strain level required for a detection remains implausibly high, as noted above. In contrast, only a small crustal strain would have been required to have produced a detectable level of gravitational-wave emission from the recycled pulsars, which, together with surpassing the spin-down limit for our recycled pulsars, indicates that we are entering new territory in terms of the physical requirements for a detection.

Assuming instead distortion by a strong internal magnetic field $B_{\rm int}$ in a superconducting core, we can use the results of Lander et al. (2012), Mastrano & Melatos (2012), and Lander (2014):

$$\epsilon \approx 10^{-8}\frac{B_{\rm int}}{10^{12}\ {\rm G}}. \tag{10}$$

See also de Araujo et al. (2016, 2017) for another study related to distortion by a strong internal magnetic field for pulsars with known braking indices. For the Crab pulsar, this corresponds to a (nonrestricted prior) upper limit on the internal field of $B_{\rm int} \approx 8.6 \times 10^{14}$ G. This can be compared with the values of the *external field*, as estimated assuming 100% electromagnetic dipole spin-down, of $B_{\rm ext} \approx 3.8 \times 10^{12}$ G, as taken from the ATNF Pulsar Catalog (Manchester et al. 2005); i.e., we can say that the internal magnetic field is no more than about 230 times stronger than the inferred external field. Similarly, for J0711−6830 we have an upper limit $B_{\rm int} \approx 7.2 \times 10^{11}$ G, to be compared with the inferred $B_{\rm ext} \approx 2.9 \times 10^{8}$ G; i.e., we can say the internal field is no more than about 2500 times stronger than the inferred external field. As noted above, a significantly larger internal field than external is possible, if field burial takes place during a previous accretion phase. This would also require that the field is stable and remains buried over the lifetime of the star; see Mukherjee (2017) for a recent review of relevant issues for millisecond pulsars (MSPs).

As in previous analyses (Abbott et al. 2017d, 2019a), we have constrained the gravitational-wave emission from the Crab pulsar. For the Crab pulsar, we have set the upper limit on its ellipticity of $\approx 8.6 \times 10^{-6}$. While significantly larger than the ellipticity upper limits we have set for the recycled pulsars, this is nevertheless of considerable interest, as it represents an ellipticity of approximately 1.0×10^{-2} times the spin-down limit. Equivalently, we can say that our non-detection implies that a fraction of no more than 1.0×10^{-4} of the Crab pulsar's spin-down energy is going into the gravitational-wave channel. For the Vela pulsar, we have set a best upper limit of 1.2×10^{-4} on its ellipticity, which is 6.6×10^{-2} times its spin-down limit, showing that no more than 4.4×10^{-3} of its spin-down energy is going into the gravitational-wave channel. Clearly, on energetic grounds, there was ample scope for making a detection, even if the required ellipticities themselves were comparatively large.

The other results presented, including those of the narrow-band search, give slightly fewer constraining upper limits on the gravitational-wave amplitudes, with corresponding small changes in the inferred upper limits on ellipticity and fraction of energy going into the gravitational-wave channel.

6. Conclusions

In this paper, we have presented two main results. We have reported new gravitational-wave upper limits on the gravitational-wave emission from the MSPs J0437−4715 and J0711−6830, matching or surpassing their spin-down limits. These limits represent a significant milestone for gravitational-wave astronomy, as this is the first time our direct gravitational-wave observations provide limits at or below the spin-down limit for an MSP. We have also reported updated limits on the fraction of spin-down energy going into the gravitational-wave channel for two young pulsars: the Crab and Vela pulsars.

Recently, Woan et al. (2018) noted a lack of pulsars at the bottom left of the pulsar period–period derivative diagram, i.e., a deficit in pulsars with high spin frequencies and small spin-down rates. Woan et al. (2018) noted that this could be a consequence of the existence of a gravitational-wave spin-down connected with a universal minimum ellipticity in MSPs of $\epsilon \approx 10^{-9}$. Reaching the level of sensitivity required to obtain a limit of $\epsilon \approx 10^{-9}$ for J0711−6830 is not trivial with second-generation detectors. This would require the planned network of five advanced detectors to reach their design sensitivity (Abbott et al. 2018b), and collect data for times exceeding at least 1–1.5 yr of observation. On the other hand, that ellipticity level will be accessible to third-generation detectors such as the Einstein Telescope (Punturo et al. 2010) and Cosmic Explorer (Reitze et al. 2019).

The gravitational-wave data used here were drawn from the O1, O2, and O3 runs of the Advanced LIGO and Advanced Virgo detectors. More data have been taken since, which will allow us to probe deeper still into the gravitational-wave emission of spinning neutron stars. Also, the analysis reported here involved five particularly interesting targets. The full LIGO and Virgo data sets can be brought to bear on many more known pulsars. Such an analysis is underway, and will be reported at a later date.

The authors gratefully acknowledge the support of the United States National Science Foundation (NSF) for the construction and operation of the LIGO Laboratory and Advanced LIGO as well as the Science and Technology Facilities Council (STFC) of the United Kingdom, the Max-Planck-Society (MPS), and the State of Niedersachsen/Germany for support of the construction of Advanced LIGO and construction and operation of the GEO600 detector. Additional support for Advanced LIGO was provided by the Australian Research Council. The authors gratefully acknowledge the Italian Istituto Nazionale di Fisica Nucleare (INFN), the French Centre National de la Recherche Scientifique (CNRS), and the Netherlands Organization for Scientific Research, for the construction and operation of the Virgo detector and the creation and support of the EGO consortium. The authors also gratefully acknowledge research support from these agencies as well as by the Council of Scientific and Industrial Research of India, the Department of Science and Technology, India, the Science & Engineering Research Board (SERB), India, the Ministry of Human Resource Development, India, the Spanish Agencia Estatal de Investigación, the Vicepresidència i Conselleria d'Innovació Recerca i Turisme and the Conselleria d'Educació i Universitat del Govern de les Illes Balears, the Conselleria d'Innovació Universitats,

Ciència i Societat Digital de la Generalitat Valenciana and the CERCA Programme Generalitat de Catalunya, Spain, the National Science Centre of Poland, the Swiss National Science Foundation (SNSF), the Russian Foundation for Basic Research, the Russian Science Foundation, the European Commission, the European Regional Development Funds (ERDF), the Royal Society, the Scottish Funding Council, the Scottish Universities Physics Alliance, the Hungarian Scientific Research Fund (OTKA), the French Lyon Institute of Origins (LIO), the Belgian Fonds de la Recherche Scientifique (FRS-FNRS), Actions de Recherche Concertés (ARC) and Fonds Wetenschappelijk Onderzoek—Vlaanderen (FWO), Belgium, the Paris Île-de-France Region, the National Research, Development and Innovation Office Hungary (NKFIH), the National Research Foundation of Korea, Industry Canada and the Province of Ontario through the Ministry of Economic Development and Innovation, the Natural Science and Engineering Research Council Canada, the Canadian Institute for Advanced Research, the Brazilian Ministry of Science, Technology, Innovations, and Communications, the International Center for Theoretical Physics South American Institute for Fundamental Research (ICTP-SAIFR), the Research Grants Council of Hong Kong, the National Natural Science Foundation of China (NSFC), the Leverhulme Trust, the Research Corporation, the Ministry of Science and Technology (MOST), Taiwan, and the Kavli Foundation. The authors gratefully acknowledge the support of the NSF, STFC, INFN, and CNRS for provision of computational resources.

We would like to thank all of the essential workers who put their health at risk during the COVID-19 pandemic, without whom we would not have been able to complete this work.

Software: The parameter estimation was performed with the LALINFERENCE (Veitch et al. 2015) library within LALSUITE (LIGO Scientific Collaboration 2018). All plots have been prepared using Matplotlib (Hunter 2007).

References

Aasi, J., Abadie, J., Abbott, B. P., et al. 2014, ApJ, 785, 119
Aasi, J., Abbott, B. P., Abbott, R., et al. 2015, CQGra, 32, 074001
Abadie, J., Abbott, B. P., Abbott, R., et al. 2011, ApJ, 737, 93
Abbott, B., Abbott, R., Adhikari, R., et al. 2008, ApJL, 683, L45
Abbott, B. P., Abbott, R., Abbott, T. D., et al. 2017a, PhRvL, 119, 161101
Abbott, B. P., Abbott, R., Abbott, T. D., et al. 2017b, Natur, 551, 85
Abbott, B. P., Abbott, R., Abbott, T. D., et al. 2017c, ApJL, 848, L12
Abbott, B. P., Abbott, R., Abbott, T. D., et al. 2017d, ApJ, 839, 12
Abbott, B. P., Abbott, R., Abbott, T. D., et al. 2017e, PhRvD, 96, 122006
Abbott, B. P., Abbott, R., Abbott, T. D., et al. 2018a, PhRvL, 121, 161101
Abbott, B. P., Abbott, R., Abbott, T. D., et al. 2018b, LRR, 21, 3
Abbott, B. P., Abbott, R., Abbott, T. D., et al. 2019a, ApJ, 879, 10
Abbott, B. P., Abbott, R., Abbott, T. D., et al. 2019b, PhRvD, 99, 122002
Abbott, B. P., Abbott, R., Abbott, T. D., et al. 2019c, PhRvX, 9, 031040
Abbott, B. P., Abbott, R., Abbott, T. D., et al. 2019d, PhRvD, 100, 104036
Abbott, B. P., Abbott, R., Abbott, T. D., et al. 2019e, arXiv:1908.06060
Abbott, B. P., Abbott, R., Abbott, T. D., et al. 2019f, ApJ, 875, 122
Abbott, B. P., Abbott, R., Abbott, T. D., et al. 2019g, PhRvD, 100, 024004
Abbott, B. P., Abbott, R., Abbott, T. D., et al. 2020a, ApJ, 899, 170
Abbott, B. P., Abbott, R., Abbott, T. D., et al. 2020b, ApJL, 892, L3
Abbott, R., Abbott, T. D., Abraham, S., et al. 2019h, arXiv:1912.11716
Acernese, F., Agathos, M., Agatsuma, K., et al. 2015, CQGra, 32, 024001
Acernese, F., Agathos, M., Aiello, L., et al. 2019, PhRvL, 123, 231108
Alford, M. G., & Schwenzer, K. 2015, MNRAS, 446, 3631
Astone, P., Colla, A., D'Antonio, S., Frasca, S., & Palomba, C. 2012, JPhCS, 363, 012038
Astone, P., D'Antonio, S., Frasca, S., & Palomba, C. 2010, CQGra, 27, 194016
Baiko, D. A., & Chugunov, A. I. 2018, MNRAS, 480, 5511
Bailes, M., Jameson, A., Flynn, C., et al. 2017, PASA, 34, e045
Baym, G., & Pines, D. 1971, AnPhy, 66, 816
Bildsten, L. 1998, ApJL, 501, L89
de Araujo, J. C. N., Coelho, J. G., & Costa, C. A. 2016, ApJ, 831, 35
de Araujo, J. C. N., Coelho, J. G., & Costa, C. A. 2017, EPJC, 77, 350
Deller, A. T., Bailes, M., & Tingay, S. J. 2009, Sci, 323, 1327
Dodson, R., Legge, D., Reynolds, J. E., & McCulloch, P. M. 2003, ApJ, 596, 1137
Dupuis, R. J., & Woan, G. 2005, PhRvD, 72, 102002
Ellis, J. A., Vallisneri, M., Taylor, S. R., & Baker, P. T. 2019, ENTERPRISE: Enhanced Numerical Toolbox Enabling a Robust PulsaR Inference SuitE, Zenodo, doi:10.5281/zenodo.4059815
Fattoyev, F. J., Horowitz, C. J., & Lu, H. 2018, arXiv:1804.04952
Fishbach, M., Gray, R., Magaña Hernandez, I., et al. 2019, ApJL, 871, L13
Gancio, G., Lousto, C. O., Combi, L., et al. 2020, A&A, 633, A84
Glampedakis, K., & Gualtieri, L. 2018, in The Physics and Astrophysics of Neutron Stars, Astrophysics and Space Science Library, Vol. 457, ed. L. Rezzolla et al. (Dordrecht: Springer), 673
Glendenning, N. K. 1996, Compact Stars. Nuclear Physics, Particle Physics and General Relativity (New York: Springer)
Hobbs, G. B., Edwards, R. T., & Manchester, R. N. 2006, MNRAS, 369, 655
Horowitz, C. J., & Kadau, K. 2009, PhRvL, 102, 191102
Hunter, J. D. 2007, CSE, 9, 90
Isi, M., Pitkin, M., & Weinstein, A. J. 2017, PhRvD, 96, 042001
Jaranowski, P., & Królak, A. 2010, CQGra, 27, 194015
Jaranowski, P., Królak, A., & Schutz, B. F. 1998, PhRvD, 58, 063001
Jones, D. I. 2010, MNRAS, 402, 2503
Jones, D. I. 2015, MNRAS, 453, 53
Jones, D. I., & Andersson, N. 2002, MNRAS, 331, 203
Kaplan, D. L., Chatterjee, S., Gaensler, B. M., & Anderson, J. 2008, ApJ, 677, 1201
Kerr, M., Reardon, D. J., Hobbs, G., et al. 2020, PASA, 37, e020
Lander, S. K. 2014, MNRAS, 437, 424
Lander, S. K., Andersson, N., & Glampedakis, K. 2012, MNRAS, 419, 732
Lentati, L., Alexander, P., Hobson, M. P., et al. 2014, MNRAS, 437, 3004
LIGO Scientific Collaboration 2018, LIGO Algorithm Library, Caltech Library
Lyne, A. G., Jordan, C. A., Graham-Smith, F., et al. 2015, MNRAS, 446, 857
Manchester, R. N., Hobbs, G., Bailes, M., et al. 2013, PASA, 30, e017
Manchester, R. N., Hobbs, G. B., Teoh, A., & Hobbs, M. 2005, AJ, 129, 1993
Mastrano, A., & Melatos, A. 2012, MNRAS, 421, 760
Mastrogiovanni, S., Astone, P., D'Antonio, S., et al. 2017, CQGra, 34, 135007
McKee, J. W., Lyne, A. G., Stappers, B. W., Bassa, C. G., & Jordan, C. A. 2018, MNRAS, 479, 4216
Mukherjee, D. 2017, JApA, 38, 48
Ng, C.-Y., & Romani, R. W. 2004, ApJ, 601, 479
Ng, C.-Y., & Romani, R. W. 2008, ApJ, 673, 411
Osborne, E. L., & Jones, D. I. 2020, MNRAS, 494, 2839
Owen, B. J. 2005, PhRvL, 95, 211101
Pedregosa, F., Varoquaux, G., Gramfort, A., et al. 2011, Journal of Machine Learning Research, 12, 2825
Piccinni, O. J., Astone, P., D'Antonio, S., et al. 2019, CQGra, 36, 015008
Pitkin, M., Gill, C., Jones, D. I., Woan, G., & Davies, G. S. 2015, MNRAS, 453, 4399
Pitkin, M., Isi, M., Veitch, J., & Woan, G. 2017, arXiv:1705.08978v1
Punturo, M., Abernathy, M., Acernese, F., et al. 2010, CQGra, 27, 084007
Ransom, S. M., Eikenberry, S. S., & Middleditch, J. 2002, AJ, 124, 1788
Reardon, D. J., Hobbs, G., Coles, W., et al. 2016, MNRAS, 455, 1751
Reitze, D., Adhikari, R. X., Ballmer, S., et al. 2019, BAAS, 51, 35
Shaw, B., Lyne, A. G., Stappers, B. W., et al. 2018, MNRAS, 478, 3832
Shaw, B., Mickaliger, M., Keith, M., et al. 2019, ATel, 12957, 1
Shklovskii, I. S. 1970, SvA, 13, 562
Singh, N., Haskell, B., Mukherjee, D., & Bulik, T. 2020, MNRAS, 493, 3866
Sun, L., Goetz, E., Kissel, J. S., et al. 2020, Characterization of Systematic Error in Advanced LIGO Calibration, Tech. Rep., LIGO-P1900245
Tse, M., Yu, H., Kijbunchoo, N., et al. 2019, PhRvL, 123, 231107
Ushomirsky, G., Cutler, C., & Bildsten, L. 2000, MNRAS, 319, 902
Vallisneri, M., Kanner, J., Williams, R., Weinstein, A., & Stephens, B. 2015, JPhCS, 610, 012021
Veitch, J., Raymond, V., Farr, B., et al. 2015, PhRvD, 91, 042003
Veitch, J., & Vecchio, A. 2010, PhRvD, 81, 062003
Vigelius, M., & Melatos, A. 2009, MNRAS, 395, 1963
Woan, G., Pitkin, M. D., Haskell, B., Jones, D. I., & Lasky, P. D. 2018, ApJL, 863, L40
Yao, J. M., Manchester, R. N., & Wang, N. 2017, ApJ, 835, 29
Zimmermann, M., & Szedenits, E., Jr. 1979, PhRvD, 20, 351